NASA/CR—2001-210687 AIAA–2001–0230

Use of a Scale Model in the Design of Modifications to the NASA Glenn Icing Research Tunnel

Victor A. Canacci, Jose C. Gonsalez, and David A. Spera
Dynacs Engineering Company, Inc., Brook Park, Ohio

March 2001

The NASA STI Program Office . . . in Profile

Since its founding, NASA has been dedicated to the advancement of aeronautics and space science. The NASA Scientific and Technical Information (STI) Program Office plays a key part in helping NASA maintain this important role.

The NASA STI Program Office is operated by Langley Research Center, the Lead Center for NASA's scientific and technical information. The NASA STI Program Office provides access to the NASA STI Database, the largest collection of aeronautical and space science STI in the world. The Program Office is also NASA's institutional mechanism for disseminating the results of its research and development activities. These results are published by NASA in the NASA STI Report Series, which includes the following report types:

- TECHNICAL PUBLICATION. Reports of completed research or a major significant phase of research that present the results of NASA programs and include extensive data or theoretical analysis. Includes compilations of significant scientific and technical data and information deemed to be of continuing reference value. NASA's counterpart of peer-reviewed formal professional papers but has less stringent limitations on manuscript length and extent of graphic presentations.

- TECHNICAL MEMORANDUM. Scientific and technical findings that are preliminary or of specialized interest, e.g., quick release reports, working papers, and bibliographies that contain minimal annotation. Does not contain extensive analysis.

- CONTRACTOR REPORT. Scientific and technical findings by NASA-sponsored contractors and grantees.

- CONFERENCE PUBLICATION. Collected papers from scientific and technical conferences, symposia, seminars, or other meetings sponsored or cosponsored by NASA.

- SPECIAL PUBLICATION. Scientific, technical, or historical information from NASA programs, projects, and missions, often concerned with subjects having substantial public interest.

- TECHNICAL TRANSLATION. English-language translations of foreign scientific and technical material pertinent to NASA's mission.

Specialized services that complement the STI Program Office's diverse offerings include creating custom thesauri, building customized data bases, organizing and publishing research results . . . even providing videos.

For more information about the NASA STI Program Office, see the following:

- Access the NASA STI Program Home Page at ***http://www.sti.nasa.gov***

- E-mail your question via the Internet to help@sti.nasa.gov

- Fax your question to the NASA Access Help Desk at 301–621–0134

- Telephone the NASA Access Help Desk at 301–621–0390

- Write to:
  NASA Access Help Desk
  NASA Center for AeroSpace Information
  7121 Standard Drive
  Hanover, MD 21076

NASA/CR—2001-210687 AIAA–2001–0230

Use of a Scale Model in the Design of Modifications to the NASA Glenn Icing Research Tunnel

Victor A. Canacci, Jose C. Gonsalez, and David A. Spera
Dynacs Engineering Company, Inc., Brook Park, Ohio

Prepared for the
39th Aerospace Sciences Meeting and Exhibit
sponsored by the American Institute of Aeronautics and Astronautics
Reno, Nevada, January 8–11, 2001

Prepared under Contract NAS3–98008

National Aeronautics and
Space Administration

Glenn Research Center

March 2001

Available from

NASA Center for Aerospace Information
7121 Standard Drive
Hanover, MD 21076
Price Code: A03

National Technical Information Service
5285 Port Royal Road
Springfield, VA 22100
Price Code: A03

Available electronically at http://gltrs.grc.nasa.gov/GLTRS

USE OF A SCALE MODEL TUNNEL IN THE DESIGN OF MODIFICATIONS TO THE NASA-GLENN ICING RESEARCH TUNNEL

Victor A. Canacci, Jose C. Gonsalez, and David A. Spera
Dynacs Engineering Company, Inc.
Brook Park, Ohio 44142

Abstract

Major modifications were made in 1999 to the 6-ft by 9-ft (1.8-m by 2.7-m) Icing Research tunnel (IRT) at the NASA Glenn Research Center, including replacement of its heat exchanger and associated ducts and turning vanes, and the addition of fan outlet guide vanes (OGVs). A one-tenth scale model of the IRT (designated as the SMIRT) was constructed with and without these modifications and tested to increase confidence in obtaining expected improvements in flow quality around the tunnel loop. The SMIRT is itself an aerodynamic test facility whose flow patterns without modifications have been shown to be accurate, scaled representations of those measured in the IRT prior to the 1999 upgrade program. In addition, tests in the SMIRT equipped with simulated OGVs indicated that these devices in the IRT might reduce flow distortions immediately downstream of the fan by two thirds.

Flow quality parameters measured in the SMIRT were projected to the full-size modified IRT, and quantitative estimates of improvements in flow quality were given prior to construction. In this paper, the results of extensive flow quality studies conducted in the SMIRT are documented. Samples of these are then compared with equivalent measurements made in the full-scale IRT, both before and after its configuration was upgraded. Airspeed, turbulence intensity, and flow angularity distributions are presented for cross sections downstream of the drive fan, both upstream and downstream of the replacement flat heat exchanger, in the stilling chamber, in the test section, and in the wakes of the new corner turning vanes with their unique expanding and contracting designs. Lessons learned from these scale-model studies are discussed.

Nomenclature

COV	coefficient of variation of airspeed, U_{std}/U_{mean}
C, D	3rd and 4th tunnel corners downstream from test section
c	chord length of corner turning vanes
d	axial distance from vane TE plane
D	diameter of drive fan
H	height of duct
HX	heat exchanger
IRT	Icing Research Tunnel (6' x 9')
OGP	fan outlet guide plate, in the SMIRT
OGV	fan outlet guide vane, in the IRT
r	radial coordinate of polar plot (Fig. 8)
SMIRT	Scale Model Icing Research Tunnel
Station	tunnel cross-section
STD	standard deviation from the mean
TE	airfoil trailing edge
U	axial airspeed
U_{avg}	polar average axial velocity in the vent tower within a 5-deg (0.09 rad) sector
U_{mean}	mean axial airspeed in cross section
U_{std}	standard deviation of axial airspeed
u'	turbulence in axial airspeed
u'/U	axial turbulence intensity
v'	lateral turbulence in airspeed
v'/U	lateral turbulence intensity
W	width of duct
y	lateral distance from tunnel inner wall
Y	normalized lateral distance, y/W
z	vertical distance above tunnel floor
Z	normalized vertical distance, z/H
α	pitch flow angle (+ toward ceiling)
$d\alpha$	STD of pitch flow angle
β	yaw flow angle (+ toward outer wall)
$d\beta$	STD of yaw flow angle
ϕ	azimuthal coordinate (Fig. 8)
ϕ_{avg}	average of azimuths within a 5-deg (0.09 rad) sector

Introduction

Background

Research in aircraft icing and component qualification tests have been conducted in the Icing Research Tunnel (IRT) at the NASA Glenn Research Center (GRC; formerly the Lewis Research Center) for over fifty-five years.[1] A plan view of the original, or baseline, configuration of the IRT is shown schematically in **Figure 1(a).** The air flow in the supply legs, from the vent tower section downstream of the fan through the refrigeration heat exchanger and into the stilling chamber, has been shown to be unevenly distributed across duct flow areas.[2, 3] It was theorized that these flow distortions had two primary causes: (1) the uneven "W" shape of the heat exchanger, which is illustrated in **Figure 1(b),** and (2) the presence of two large fairings around the legs of the support stand below the fan motor and its nacelle, which are shown in **Figure 2.**

In 1999, NASA conducted a program of upgrades to the IRT.[4, 5] The aforementioned W-shaped heat exchanger was replaced with a flat-faced heat exchanger, changing the configuration of the C-D leg of the IRT to that shown schematically in **Figure 3.** These modifications were designed to remove much of the distortion in the flow entering the stilling chamber. To accommodate the required surface area of the flat heat exchanger, the duct between the third and fourth corners of the tunnel loop (Corners C and D) was widened from 29.2 to 49.2 feet (8.9 to 15.0 m). This added width in the C-D leg necessitated new cascades of turning vanes in Corner C (with an expansion ratio of 1.7) and Corner D (with a contraction ratio of 0.6).

In addition to these modifications to the C-D leg, outlet guide vanes (OGVs) were added to the fan drive assembly, in an effort to efficiently remove as much swirl and angularity as possible from the outflow of the fan. The original fan drive had inlet guide vanes to pre-swirl the airflow entering the fan, but no OGVs to straighten the flow leaving the fan.

Objectives of the Scale Model Program

A 1/10 th scale model of the IRT, designated as the SMIRT and shown in **Figures 4(a)** to **(g),** was constructed and tested for the purpose of reducing the technical risk associated with making these major changes to the IRT.[6] Flow quality was measured at all critical sections of this scale model wind tunnel with the objectives of (1) validating the aerodynamic designs of the new corner turning vanes, and (2) providing quantitative predictions of the expected improvements in the uniformity of the flow entering the new heat exchangers, the spraybars, and the Test Section of the full-scale IRT after its modification. Additional goals of this effort were to (3) identify any potential flow problems with the new OGVs, heat exchangers, and turning vanes, (4) provide flow quality data at locations where it was not possible or practical to perform full-scale measurements, and (5) avoid the high costs of full-scale testing and interference with the very full research test schedule of the IRT.

SMIRT Program

The SMIRT test program was conducted in two parts. The first part consisted of tests, which qualified the SMIRT as an accurate representation of the IRT with regard to flow patterns.[7] The SMIRT was first configured to model the original or baseline IRT, to verify that flow distortions occurring in the SMIRT correlate satisfactorily with those measured in the unmodified IRT. This verification was particularly important because full-scale airspeeds were modeled in the SMIRT and not Reynolds numbers.

The tunnel station (cross-section) selected for this comparison was in the vent tower section, between the fan motor nacelle and Corner C (Fig. 1). Flow distortions measured in the SMIRT were found to correlate closely with those measured previously in the IRT. The first part of this study concluded with the widening of the C-D leg of the SMIRT to the new configuration shown in Figure 3, and with the installation of scale models of the new flat heat exchanger, the new C- and D-Corner turning vanes, and flat outlet guide plates (OGPs) to simulate the airfoil OGVs in the IRT. Tests with plates of different lengths were then conducted to determine the length needed to straighten the outflow of the fan to the degree expected in the IRT.

The second part of the program consisted of a series of flow-quality measurements made at key sections in the SMIRT in its fully-modified configuration, which were then projected to the full-scale IRT.[8] These sections are located in the Vent Tower down-stream of the fan, upstream and downstream of the new flat heat exchangers, in the Stilling Chamber upstream of the spray bars, in the Test Section, and in the wakes of the new turning vanes in Corners C and D.

Comparison of IRT and SMIRT Flow Qualities

In this paper, recent measurement of flow quality in the vent tower, stilling chamber, and test sections of the full-scale modified IRT are compared with projections based on SMIRT test data. The objective of this final phase of the SMIRT program is to present an assessment of the accuracy of these projections, together with an evaluation of model details and lessons learned during the course of the program.

Reynolds Number Considerations

Flow quality testing in the SMIRT was conducted at the same airspeeds as testing in the IRT, so Reynolds numbers in the SMIRT tests were only one-tenth those in the IRT. For example, when the tunnel's characteristic length is taken as the square root of the test section flow area and the test section airspeed is 350 mph (156 m/s), the SMIRT Reynolds number is approximately 2.6×10^6, compared to 26×10^6 for an IRT test at the same airspeed. In this study it was assumed that accurate modeling of flow distortions, particularly in the low-speed ducts of the tunnel, depended more on accurate modeling of internal geometric shapes than on equality of Reynolds numbers.

Recent measurements of flow quality in the IRT test section, however, showed that airspeed and turbulence do change with Reynolds number, while flow angles are not significantly affected. [9] Axial airspeed variations (coefficients of variation and turbulence) increased somewhat as the tunnel Reynolds numbers was decreased by a factor of 3. Therefore, airspeed and flow angle variations measured in the modified IRT were expected to be equal to or less than the equivalent parameters measured in the SMIRT, because of neutral-to-favorable Reynolds number effects.

Summary of Flow Qualities Measured in the IRT and SMIRT

After modifications to the IRT were complete, flow quality surveys were conducted at Station 2 (Vent Tower, downstream of the fan), Station 5 (Stilling Chamber, upstream of the spraybars), and Station 6 (mid-length in the Test Section).[10, 11] In **Table 1**, averages of flow qualities at these stations in the IRT, before and after modification, are compared with measurements on the modified SMIRT. SMIRT data with both long and short OGPs are included where available.

Comparison of the results for the modified IRT with those before modification show that there were improvements in all parameters in the Vent Tower and the Stilling Chamber at the inlet to the spraybars. Moreover, the scale of each improvement is generally the same as that projected from the SMIRT data.

In the Test Section, the SMIRT data are a lower bound on flow variations, because of the absence of spraybars. In the IRT, flow quality remained the same except for the coefficient of variation of airspeed in the core zone. The latter parameter increased from 0.2 to 0.3 percent.

Description of the SMIRT Test Facility

Baseline IRT Configuration

The SMIRT facility was designed and fabricated at NASA's Glenn Research Center (formerly the Lewis Research Center) beginning in 1991. This one-tenth scale model of the IRT was designed to be modular, so flow-conditioning devices or entire sections of the tunnel can be easily installed and removed. The majority of the loop sections were fabricated using 0.5 in. (13 mm) thick clear acrylic walls supported by rectangular aluminum frames, as shown in **Figure 4(a).** Constant-area sections exist from the vent tower section upstream of Corner C to the Stilling Chamber, downstream of Corner D, with a width W of 35.0 in. (889 mm) and a height H of 31.4 in. (797 mm). A 14:1 contraction section, fabricated from welded aluminum sheets, connects the Stilling Chamber to the Test Section. The Test Section is 24 in. (609 mm) long, 10.8 in. (274 mm) wide, and 7.2 in. (183 mm) high. Maximum air speed in the SMIRT Test Section is 550 ft/s (168 m/s).

Two diffusing sections, from the Test Section to Corner A and from Corner A to Corner B, decelerate the airflow while connecting the Test Section to the fan leg. The fan leg, between Corners B and C, consists of four components: (1) an inlet transition section, (2) a circular section 30 in. (762 mm) diameter surrounding the fan, (3) an outlet transition section, and (4) the Vent Tower section. The transition and circular sections are fabricated from fiberglass that is finished on the inner walls, and supported by a wooden framework on the outside of the tunnel.

The Vent Tower section is vented to the test cell containing the SMIRT, producing an internal static pressure that is slightly above atmospheric. The Vent Tower section was originally fabricated from 0.5 in. (127 mm) acrylic sheets, with 0.25 in. (6.4 mm) acrylic doors that could be moved toward the center of the section to allow venting. However, in order to support the large actuators required to hold and traverse the hot-wire probes used to measure air velocities, the acrylic walls were replaced with 0.5 in. (13 mm) aluminum plates mounted inside aluminum frames. Venting to atmosphere is now accomplished through rectangular openings on both sidewalls, which are 3.5 in (89 mm) wide and 8.0 in. (203 mm) high and covered on the outside by flexible flaps. These outward-opening flaps model two personnel access doors in the IRT that swing open during fan operation to provide relief of internal pressure.

The turning vanes in the baseline configuration of the SMIRT were machined from phenolic tubing and

mounted to aluminum structures. The distinctive W-shaped heat exchanger (Fig. 1(b)) was constructed as an aerodynamic model only. The large manifolds in the bends of the "W" were modeled with solid wood fairings, while the tube banks were simulated with a 4-mesh screen, with four 0.035 in (9 mm) diameter wires per inch (25 mm). During checkout testing, it was determined that this screen size was too coarse to produce flow patterns immediately downstream that accurately represented the flow in the IRT in the same area. Therefore, only measurements of flow distortion upstream of the heat exchanger where used to qualify the SMIRT facility during the first part of this study.

The eight horizontal spray bars in the IRT at the time the SMIRT was designed were modeled by 0.75 in. (19 mm) diameter solid aluminum cylinders, while the three vertical supports were machined to an airfoil shape from aluminum bar stock. This spray bar model was removed entirely from the modified SMIRT, because the set of ten airfoil-shaped spray bars recently installed in the IRT have much lower drag coefficients than the round bars in the model.

Expanded C-D Leg Configuration

After the SMIRT flow was qualified as an accurate representation of the IRT flow in the vent tower section, the baseline C-D leg was removed and a new C-D leg was installed to model the modified IRT configuration that is illustrated in Figure 3. This wider leg, shown in **Figure 4(b)**, was fabricated out of 3/16-in. (48 mm) aluminum sheets riveted to aluminum frames.

Sixteen custom-designed turning vanes were installed in Corner C to expand the flow by a factor of 1.7, and sixteen vanes were installed in Corner D to contract the flow by a factor of 0.6. Each new turning vane was cast in one piece from a polyurethane-epoxy material around an internal aluminum bar which was bolted to the tunnel floor and ceiling.

Although each model turning vane was fabricated in one piece (from floor to ceiling) the new turning vanes in the IRT were actually built up in three segments. Each vane had a flanged and bolted joint at 1/3 and 2/3 of its height. A continuous horizontal tie plate was sandwiched between the flanges at each of these joints and anchored to the tunnel's inner wall. The tie plates were designed to carry diagonal airloads on the vanes, and the segmented construction reduced overall fabrication costs. As will be discussed later, the tie plates and flanges produced flow distortions that were not found in the SMIRT.

Fan and Nacelle

A 12-bladed, 30 in. (762 mm) diameter fan shown in **Figure 4(c)** drives airflow around the SMIRT circuit. Fan blades were machined from aluminum to match the Clark Y profiles, twist, and taper of the laminated wood blades in the IRT fan. The blades are held in place on an aluminum hub by two aluminum disks. The nacelle and support-leg fairings were fabricated from fiberglass, while the support legs, the turbine shaft, and other structural components inside the nacelle were fabricated from carbon steel.

The fan is powered by a commercially available four-stage air turbine motor with a 0-to-450 psia (0-to-3,100 kPa) air supply. [12]. The SMIRT fan rotates at speeds up to 4,500 rpm (488 rad/s). Tests discussed in this paper were performed at a fan speed of approximately 4,400 rpm (461 rad/s), which produces a test section airspeed of 350 mph (156 m/s). At this speed the fan uses approximately 3.5 lbm/s (1.6 kg/s) of air and generates approximately 60 hp (45 kW). Remotely controlled globe valves regulate the airflow to the turbine. Turbine air is conditioned to 120 F (35 C) using a steam heat exchanger. The exhaust of the air turbine is vented out of the nacelle through hollow support legs and into the surrounding test cell. Test section velocities and Mach numbers are calculated on-line from the total pressure, static pressure, and total temperature measured in the test section. Safety systems close the globe valves supplying the turbine air if tunnel temperatures, shaft bearing temperatures, shaft speeds, or vibrations exceed allowable limits.

Simulated Outlet Guide Vanes

The 12 outlet guide vanes (OGVs) installed around the fan motor nacelle in the modified IRT are cambered and twisted airfoils with constant chord lengths of 6.0 ft (1.8 m), or 0.24 *D*, where *D* is the fan diameter of 25.5 ft (7.8 m). Accurate modeling of these complex airfoils was not cost-effective, so the expected flow-straightening effect of the IRT OGVs was simulated with five flat plates, as shown in **Figures 4(d)** and **(e)**. These outlet guide plates (OGPs) and the two nacelle support legs were spaced approximately 51 deg apart.

Two plate chord lengths were tested to determine the minimum length required to satisfactorily eliminate most of the swirl effects in the fan outflow. The shorter plates, shown in Figure 4(d), were 18 in. (457 mm) in chord length (0.6 *D*, where *D* is the diameter of the drive fan) and were fabricated from 0.5 in. (13 mm) thick wood covered with several layers of fiberglass. An epoxy-based paint provided a smooth finish. The OGPs were held in place on the motor nacelle by a U-shaped track, and several screws attached each baffle to the outer wall of the tunnel. After Vent Tower flow patterns with the shorter plates were determined, the plates were extended to the length of the leg fairings, which is 42 in. (1,067 mm) or 1.4 *D*. These longer OGPs are shown in Figure 4(e). Extensions were

fabricated from 0.5 in. (13 mm) particleboard and attached to the trailing edges of the shorter baffles.

The results of the OGP length tests are summarized in the lower part of **Table 2**. Turbulence intensity and flow angularity are minimized at an *L*/D ratio of approximately 1.0. The coefficient of variation continues to decrease with increasing plate length. On the basis of these test results, it was decided to use the longer OGPs for the remaining flow quality tests, with the expectation that the actual airfoil OGVs would produce similar flow straightening and uniformity in the Vent Tower.

Sliding Mount for Instrument Probes in Test Section

An innovation that was very successful in improving the repeatability of data measured in the tunnel test section was the sliding mount for the actuator, which traverses instrument sensors in the vertical direction. This mount assembly is shown in Figures 4(f) and (g). The inserts in Figure 4(g) show a five-hole probe and a single-sensor hot-wire probe in place. Once the actuator is positioned to be perpendicular to the slide the probe is fixed parallel to the tunnel axis. The assembly can then be moved laterally across a given station or axially from station to station without disconnecting and re-connecting the actuator. Thus, changes in the probe's axial alignment, as it is moved from point to point and station to station, are virtually eliminated with this mounting system.

Flat Heat Exchanger

Two commercially available fin-tube heat exchangers were placed in a staggered arrangement in this wider tunnel leg as shown in Figures 3 and 4(b). This offset design was selected for the IRT in order to provide access for maintenance on the end turns of the coolant tubes in each assembly, without significantly increasing the width of the C-D duct. If the two assemblies were aligned an access space between them would be needed, which would require the width of the C-D leg to be increased even further in order to obtain the same heat-exchanger flow area. Each of the SMIRT heat exchangers is 31 in. (787 mm) high by 28.5 in. (724 mm) wide, and is comprised of 8 rows of 3/8 in. (95 mm) diameter tubes with twelve 0.008 in. (2 mm) thick fins per inch. These heat exchangers were used only as aerodynamic models in these studies and were not operated.

The numbers of tube rows and the fin separation in these heat exchangers were selected to provide the same pressure drop in the SMIRT as that expected across the new heat exchangers in the IRT.[13] Heat-exchanger pressure drop data from both the SMIRT and the IRT are shown in **Figure 5**. It can be seen from these data that the pressure drop measured across the SMIRT heat exchanger (HX) falls within the range experienced with the IRT "W" heat exchanger, with and without frost.[14] This range was used in the preliminary design of the flat heat exchanger. The SMIRT and IRT data are in close agreement, for the dry condition. Also, icing run time is seen to have little effect on the pressure loss in the IRT. However, pressure drops in both the scale-model and full-scale HXs were under predicted by about 70 percent.

As a result of selecting the SMIRT HX on the basis of pressure drop from commercially available units; the thickness of these model components is about 70 percent larger than the desired 1/10th of the thickness of the HXs to be installed in the IRT. This causes the relative distances from the new Corner C turning vanes to the HX in the SMIRT to be smaller than those in the modified IRT. Therefore, the flow distortions in the wakes of the turning vanes near the inner wall are expected to dissipate more quickly in the IRT than in the SMIRT, before entering the heat exchanger.

Because of the greater relative dissipation distance, it is expected that any flow distortions caused by the offset of the heat exchangers and by the Corner C turning vanes will be significantly smaller in the modified IRT than in the SMIRT. Nevertheless, only the measured values of axial turbulence are reduced to account for the larger dissipation distance. Other flow variation parameters at the heat-exchanger inlet station are projected to the IRT exactly as measured in the SMIRT.

Tunnel Operating Instrumentation

All data presented in this report were measured at a test airspeed of 350 mph (157 m/s), without model blockage in the Test Section. Pressures in the test section for determining tunnel airspeed were measured using a Pitot probe with outer and inner diameters of 0.125 in. (3.2 mm) and 0.055 in. (1.4 mm), respectively, and chamfered walls. The probe was positioned on the centerline of the tunnel 18 in. (457 mm) downstream of the test section inlet plane. Additionally, pressure taps of 0.020 in. (0.5 mm) diameter in the walls and floors of the tunnel sections provided static pressure values. Pressure were measured by an electronic scanning system using 5 psid (35 kPa) modules and recorded on a mainframe computer via the standard facility data acquisition system.

Temperatures at the exit of the test section, in the stilling chamber, and inside the test cell were measured using type-K thermocouples. The air turbine contains instrumentation to supply tunnel operators with bearing temperatures and shaft speed. Other instrumentation is present inside the nacelle to provide data on shaft speed, nacelle temperature, shaft bearing temperatures, and support vibration amplitudes.

Flow Quality Instrumentation

Measurements of local airspeed, flow angle, and turbulence were made with hot-wire X-probes, in which 0.00015 in. (0.0038 mm) diameter tungsten wires are oriented at +/- 45 degrees with respect to the flow direction. Each hot wire was connected to a 60 ft (18 m) low-impedance coaxial cable. Each of these anemometers was equipped with its own signal conditioner for low-pass filtering, DC offsetting, and amplifying. A four-channel 12-bit analog-to-digital converter with an input range of +/- 5 volts was used to digitize the anemometer bridge values after signal conditioning. A personal computer with commercially available software [15] was used to control the data acquisition process and to store the data. Each probe was calibrated in a free-jet facility at speeds up to 150 ft/s (46 m/s) together with its data acquisition equipment before use in the SMIRT.

Data acquisition sampling frequencies, low-pass filter frequencies, amplifier gains, and DC-offsets for the hot-wire measurements were 2,000 Hz, 500 Hz, 7, and 1 VDC, respectively. Low-pass frequencies were set at 1/4 of the sampling frequency to prevent aliasing of the data. Raw anemometer bridge voltages (before signal conditioning) for hot-wire probes typically vary between 0.8 and 1.5 V for velocities of 0 and 150 ft/s (46 m/s), respectively. A total of 12,288 data points were taken during each measurement traverse.

The hot-wire probes were mounted to a traversing mechanism that allowed data to be taken efficiently at precise locations throughout various cross-sections in the tunnel circuit. [16] Probes were mounted at the end of an actuator that allowed measurements to be made over distances of 30 in. (762 mm) vertically and 34 in. (864 mm) horizontally. Post-processing of the hot-wire probe data provided velocity profiles, flow angles, and turbulence levels. These data could then be further manipulated to determine average velocities across entire stations, standard deviations from these averages, and velocity polar plots.

In the test section, a five-hole flow-angle pressure probe and a hot-wire probe with a single sensor were used. The five-hole probe provided axial velocities and flow angles, and the hot-wire sensor provided turbulence data.

Data Acquisition Locations and Scope

Figure 6 shows the location of seven key stations around the tunnel circuit, selected from among the 15 stations where flow quality data were taken during this study. Both horizontal and vertical traverses were made with hot-wire anemometer probes at Stations 2, 3, 5, and 6, while horizontal traverses were made at Stations 3a, 4, and 5a. Horizontal and vertical traverses with 5-hole Pitot pressure probes were made across Station 6.

Flow measurements outside the Test Section were usually made at intervals of 1.0 in. (25.4 mm) along each traverse. At Stations 3a, 5, and 5a intervals were 0.25 in. (6.3 mm), in order to accurately measure local effects within the wakes of the turning vanes. All the hot-wire traverses produced measurements of axial airspeed and turbulence, and lateral (either pitch or yaw) airspeed and turbulence. Lateral flow angles, either pitch or yaw, were then calculated from the ratio of lateral-to-axial airspeeds. Pressure measurements in the Test Section with the 5-hole probe produced axial, pitch, and yaw airspeeds and pitch and yaw angles directly, at intervals of 0.25 in. (6.3 mm).

Facility Qualification Tests

Station 2 in the Vent Tower of the unmodified SMIRT and its counterpart in the IRT were selected as the measurement locations for conducting a baseline tunnel-to-tunnel comparison. The purpose of these preliminary tests was to verify that SMIRT flow patterns represent those in the IRT, both qualitatively and quantitatively. Large, asymmetric variations in airspeed have been measured in this area of the IRT, which provided a meaningful test for the SMIRT. The results of these qualification tests are shown in **Figures 7** and **8** and are summarized in the upper part of **Table 2**.

Horizontal and Vertical Traverses in Vent Towers

Figures 7(a), (b), and (c) show clearly the similarities between horizontal profiles measured in both tunnels. Axial velocities were measured in the IRT at normalized heights of $0.33H$ and $0.67H$, and in the SMIRT at $0.25H$, $0.50H$, and $0.75H$, where H is the height of the relevant duct. Although the data in the two tunnels were measured at somewhat different relative heights, the flow patterns are very similar. Data in Figure 7(a) can be compared to show that the flow variations in the lower portions of both vent tower sections are almost identical. Both tunnels have maximum velocities on centerlines of approximately 56 ft/s (17.1 m/s), trailing off to approximately 38 ft/s (11.6 m/s) on the inner wall, and to approximately 20 ft/s (6.4 m/s) near the outer wall.

Data in Figure 7(c) can be compared to show that the flow variations in the upper halves of the Vent Tower sections are also very similar. Both tunnels show nearly uniform velocity profiles of approximately 32 ft/s (9.7 m/s) for the inner halves of the Vent Tower sections, dropping off to less than 20 ft/s (6.1 m/s) near the outer walls. Comparing Figures 7(a) and (c), it is clear that in both tunnels flows near the floor are generally much faster than those near the ceiling.

Figures 7(d), (e), and (f) present axial velocity values measured in the IRT at normalized distances of $0.33W$ and $0.67W$ from the inner wall of the Vent Tower duct, and in the SMIRT at distances of $0.25W$, $0.50W$, and $0.75W$, where W is the width of the relevant duct. Again, the data were measured at somewhat different relative distances from the inner walls of the two tunnels, but the flow patterns can still be seen to be very similar. In both tunnels, the maximum velocity near the floor on the inner half of each tunnel is approximately 70 ft/s (21.3 m/s) and decreases with height to less than 30 ft/s (9.1 m/s) near the ceiling. This very large velocity gradient in the IRT is modeled well in the SMIRT.

Data in Figure 7(f) show that the flows in the outer halves of the vent tower sections are similar as well. Both show an average velocity of approximately 30 ft/s (9.1 m/s) above the centerline, a higher velocity near the floor, and a lower velocity near the ceiling. Figures 7(d) and (f) also show that flows near the inner walls of both tunnels are generally faster than those near the outer walls.

Polar Plot Representation of Traverse Data

The data trends in Figure 7 suggest a pattern of high and low velocity regions distributed circumferentially around the axial centerline of both the IRT and the SMIRT. This pattern can best be identified by means of a polar plot of the same velocity data presented in Cartesian coordinates in Figure 7. Figure 8(a) illustrates how a polar plot can be created. This figure represents a downstream view of Station 2 in the vent tower section, with the inner (south) wall of the tunnel to the left. The cross section is first divided into 5-deg (0.09 rad) sectors centered on the axial centerline. All velocity measurements with a given sector are averaged together to obtain a value designated as the U_{avg} for that sector. The sector averages are then normalized by the mean axial velocity for the total cross-section, U_{mean}. The resulting velocity ratios are then plotted on polar, with the radial coordinate $r = U_{avg} / U_{mean}$ and azimuthal angle $\phi = \phi_{avg}$, the sector average azimuthal angle.

The polar plots at Station 2 in Figure 8(b) clearly show that both the IRT and the SMIRT tunnels have a higher velocity region near the floor and directly to the left of a radial line projected downstream from the south leg of the fan nacelle. In both tunnels the velocities in this region approach twice the mean velocity of the section. The direction of fan rotation in this view is counter-clockwise and the residual whirl velocity in the fan wake is in the same direction. Therefore, the higher velocities are apparently the result of an interaction between the whirl velocity and the long wall (1.4 D in length) formed by the south leg fairing and the south wall of the motor nacelle. The opposite interaction is observed in the upper-right in this figure, where there is a region of much-reduced velocity in the lee of the north leg fairing and the north wall of the motor nacelle. It is clear from this polar plot that the SMIRT flow accurately models the IRT flow distribution downstream of the fan as it is distorted by the motor nacelle structure.

Flow-quality data averaged across Stations 2 in the SMIRT and the IRT are listed in the upper part of **Table 2**. The SMIRT axial airspeed coefficient of variation, a parameter strongly influencing the uniformity of cooling in the downstream HX, is close to that of the IRT (32 *vs* 37 percent). Average turbulence intensity and the standard deviations of both the yaw and pitch flow angles in the IRT are all accurately modeled in the SMIRT. The flow angle correlation between the SMIRT and the IRT confirms that the residual swirl in the IRT fan wake is modeled satisfactorily in the SMIRT.

On the basis of the very close agreement between the SMIRT and the IRT flow parameters across Station 2 in each Vent Tower, it is concluded that the SMIRT produces an accurate model of the flow distortions present in the IRT. Also, differences of a factor of 10 in Reynolds number do not appear to be significant. This qualifies the SMIRT as a tool for evaluating the extent to which the IRT modifications can be expected to reduce these flow distortions.

Results and Discussion

Unmodified and Modified IRT, Compared to Modified SMIRT

After modifications to the IRT were complete, flow quality surveys were conducted at Stations 2 (Vent Tower, downstream of the fan), Station 5 (Stilling Chamber, upstream of the spraybars), and 6 (mid-length in the Test Section).[10, 11] In Table 1, averages of flow qualities at these stations in the IRT, before and after modification, are compared with measurements on the modified SMIRT. SMIRT data for both long and short OGPs are included where available.

Comparison of the results for the modified IRT with those before modification show that there were improvements in all parameters in the Vent Tower and Stilling Chamber at the inlet to the spraybars. Moreover, the scale of each improvement is generally the same as that projected from the SMIRT data.

In the Test Section, the SMIRT data are a lower bound on flow variations, because of the absence of spraybars. In the IRT, flow quality remained the same except for the coefficient of variation of airspeed in the core zone. The latter parameter increased from 0.2 to 0.3 percent.

IRT Changes Estimated from Modified SMIRT Tests

Table 3 lists the flow quality parameters for the selected stations in the IRT, as averaged across each station in its baseline (original) configuration and advance estimates of these same parameters after modifications to the facility. The latter estimates are projected from the tests conducted in the SMIRT. The two columns on the left of Table 3 designate the stations studied. The remaining columns list the four parameters which are used here as measures of flow variability, as follows: (1) Axial airspeed coefficient of variation, (2) axial turbulence intensity, (3) standard deviation of pitch flow angle, and (4) standard deviation of yaw flow angle. Standard deviations of flow angles are given rather than straight averages, because flow angle averages are essentially zero in a closed duct.

This side-by-side comparison of baseline and modified variability data shows the scope of flow-quality improvements expected in the modified IRT, from the Vent Tower through the heat exchanger and into the spraybar inlet. Projected improvements in the Test Section flow quality are less dramatic but still important. Improvement in flow quality in the low-speed sections of the tunnel was expected to result in some improvement in the icing cloud uniformity. An evaluation of icing cloud improvements is a significant part of the planned activation testing of the modified IRT.

Details of the flow distributions at key stations are presented below.

Station 2: Vent Tower Area Downstream of the Fan

Figures 9(a) to **(d)** illustrate the flow distribution measured in the modified SMIRT Vent Tower, as compared with that in the SMIRT baseline configuration. It is evident that the OGPs have been very effective in reducing the maximum and minimum values of all four of these flow variability parameters. For example, the airspeed COV was reduced from a value of 41 percent without OGPs to only 14 percent with the longer OGPs in the SMIRT. This led to the conclusion that the OGVs in the IRT would perform aerodynamically as designed, significantly flattening the airspeed profile and straightening the outflow of the fan before it enters Corner C.

Stations 3a and 5a: Wakes of New Turning Vanes in Corners C and D

Figures 10(a) and **(b)** illustrate the novel airfoil contours and the wake flow patterns of the new turning vanes in Corners C and D. The vector lines represent the combined axial and lateral airspeeds at 0.25-in. (6.3-mm) intervals along horizontal traverses. In Figure 10(a), the flow remains attached to the vanes during its 69-percent expansion from the vent tower to the C-D leg. Large variations in airspeed are seen between vectors immediately downstream of the vane trailing edge and midway between vanes.

The yaw flow toward the inner wall indicates a tendency for the flow to go around the protruding corner of the outer heat exchanger. As mentioned previously, this effect will be less in the IRT because the relative distance to the outer heat exchanger will be larger and the relative misalignment of the two upstream HX faces will be smaller than in the SMIRT. In Figure 10(b), flow downstream of the Corner D turning vanes is seen to be well attached, with smaller variations in airspeed and yaw flow angles. This is to be expected because of the converging action of these vanes.

Figure 11 presents a comparison of the changes that occur in turbulence intensity as the flow passes through the two different cascades of turning vanes. Turbulence intensity is plotted against the normalized distance from an imaginary vertical plane touching the trailing edges of each vane row. The normalization lengths are the vane chords, which are 5.76 in. (146 mm) for both the C- and D-corner vanes. At Corner C, the turbulence intensity level rises sharply from its vent-tower level as the flow encounters and passes through the vane row. Downstream of the C-vanes, turbulence decays with distance, reaching the vent-tower level in about two chord lengths. A somewhat lower asymptotic level is reached after three to four chord lengths. At Corner D, however, the lower turbulence in the flow received from the heat exchanger changes little while passing through the vane row and then decays to less than half of its initial intensity after 2 to 3 chord lengths.

On the basis of these test data, the new turning vanes were predicted to perform as designed, with flows remaining attached while being turned, expanded, and contracted. Persistence of the wake defects was also predicted.

Station 3: Upstream of the Heat Exchanger in the C-D Leg

Twelve instrumentation traverses were made across Station 3 in order to accommodate the stepped surface of the heat exchanger. Four horizontal traverses were made from each of the tunnel's side walls at 3.0 in.(76 mm) upstream from each HX face. Four vertical traverses from the tunnel ceiling were also made at this same upstream distance. The normalized lateral positions for each of these traverses (y/W) were 1/8, 3/8, 5/8, and 7/8. The HX design for the modified IRT (Fig. 3) has each of the two heat exchanger assemblies, each containing four identical modules stacked vertically. The four horizontal traverses made from each wall were at the normalized heights (z/H) of 1/8, 1/3, 2/3, and 7/8, to determine the expected flow quality at the approximate mid-height of each IRT module.

The flow quality results obtained from the horizontal and vertical traverses across Station 3 are shown graphically in **Figure 12** and listed in **Table 4**. Figures 12(a) and (b) show the lateral and vertical distributions of relative axial airspeed, U/U_{mean}, in which U_{mean} is the mean value of axial airspeed measured during all twelve traverses at Station 3. Based on these SMIRT data, airspeeds are expected to be somewhat higher in the lower modules of the inner heat exchanger in the IRT, as noted in Table 4. This effect is a continuation of the distortion pattern measured previously in the Vent Tower area, but here the gradients have been reduced.

When the airspeed measurements across Station 3 are averaged according to their HX locations, it is seen that about 53 percent of the flow enters the inner heat exchanger, with about 47 percent entering the outer. Coolant flow rates are controlled separately to each of the eight heat exchanger modules in the IRT, so it is fully expected that heat-transfer compensation can be made for this relatively small inequality in airflow

Referring again to **Figure 12(a)**, the axial airspeeds near the inner wall are highly distorted by the wakes of the inner three turning vanes in Corner C. Again, the distance from these vanes to the SMIRT heat exchangers is smaller than scale. For example, the SMIRT anemometer probe was only one-half a chord length downstream from the trailing edge (TE) of the innermost vane. In the full-scale IRT, the distance from the TE of this same vane to the face of the inner heat exchanger will be 1.5 chord lengths. The decay rate illustrated in Figure 11, means that similar wake-induced distortions of the axial airspeed in the IRT are expected to be only half as large as those shown in Figure 12(a).

Figures 12(a) and (b) illustrate the effect on axial airspeed of the step at mid-width of the tunnel, which is seen as a sharp drop of 10 to 15 percent from the inner to the outer heat exchanger. The airspeed continues to drop from mid-width to the outer wall, where the airspeed is only about 75 percent of the mean. Figures 12(c) and (d) show the measured distributions of yaw and pitch flow angles at Station 3. The large negative yaw angles visible in Figure 12(c) near the middle of the duct indicate that the step in the HX structure is causing a local flow toward the inner heat exchanger. Yaw angles are positive near the outer wall, which indicates that the flow is still expanding downstream of the turning vanes. This same expansion is indicated by the pitch flow pattern in Figure 12(d), in which pitch is positive below the ceiling and negative above the floor. Diffusion into the larger flow area of the C-D leg continues to take place up to the faces of the heat exchangers.

Station 4: Heat Exchanger Outlet in the C-D Leg

The tubes and fins of the heat exchangers act like screens on the airflow and can be expected to improve the quality of the flow across the duct. Flow measurements were therefore made a short distance downstream of the SMIRT heat exchangers to determine the extent of these expected beneficial effects. Because of the small size of the inner tunnel wall and the limited length of the anemometer probe, only the outlet of the outer HX and part of the outlet of the inner HX were accessible for flow measurements.

Figures 13 and **Table 5** present the results from the four horizontal traverses that were made at Station 4. Figure 13(a) shows that the axial airspeed increases from the outer wall inward, with little height variation above the floor. Near the middle of the duct, the wake of the centerbody of the HX assembly causes a large local deficit in the airspeed. In the short segment of the traverse that was downstream of the inner HX, the airspeed appears to continue to increase with decreasing distance from the inner wall.

The limited SMIRT airspeed data obtained at Station 4 were then projected across the inner unit of the HX, as shown by the dashed line in Figure 13(a). This projection was made on the basis of several assumptions. First, the airspeed gradient increasing from the outer wall to mid-duct was assumed to continue to the inner wall. Second, the division of flow between inner and outer HXs at their outlets was assumed to be the same as at their inlets. Third, the boundary-layer reduction in airspeed at the inner wall was assumed to be the same as that measured at the outer wall. Finally, the deficit caused by the centerbody was assumed to be only one-half as severe as that measured in the SMIRT, because the aft fairing on the IRT centerbody is significantly more aerodynamic than the blunt aft fairing in the SMIRT.

Figure 13(b) shows the lateral distribution of measured and projected yaw flow angles across the HX outlets. These are generally small, except for the flow in the wake of the HX centerbody. Angular flow distortions in the IRT in this area were projected to be only one-half of those measured, because of the improved aerodynamic shape of the full-scale HX aft fairing. Lateral flow was assumed to be symmetric with respect to the center plane of the duct, so yaw flow angles downstream of the inner HX were projected to be the negative of those measured downstream of the inner HX.

Station 5: Spray Bar Inlet Plane in the Stilling Chamber

Uniformity of the flow entering the spray bar section of the IRT is critical to the uniformity of the test section icing cloud. Therefore, one of the main reasons for modifying the IRT is to improve the quality of the airflow at Station 5, leading into the spray bars. The SMIRT tests showed that major improvements in the uniformity of airspeed across Station 5 could be expected in the modified IRT, as shown graphically in **Figures 14(a)** to **(d)**. In Figure 14(a), the large periodic variations from floor to ceiling in the baseline IRT, which were caused by the wakes of components in the "W"-shaped heat exchanger, are completely eliminated in the modified SMIRT. This figure shows dramatically the flow benefits of the flat heat exchangers.

The flow angularity distributions shown in Figures 14(b) and (d) indicate that the flow is continuing to expand slightly toward the walls, floor, and ceiling. However, flow angularity is less than 1.0 deg in both pitch and yaw in most of the duct.

Figure 14(c) presents a comparison of the lateral distributions of axial airspeed before and after installation of the flat HX. Baseline variations of almost +/-50 percent were projected to be almost completely eliminated with the flat HX. The modified airspeed distribution in the SMIRT increases somewhat from outer wall to inner wall, as was observed previously in the flow at the heat exchanger. Some flow distortions are noted near the inner wall from the wakes of the nearest turning vanes, and the flow deficit from the HX centerbody is still noticeable in the middle of the duct.

Table 6 lists the results of the flow quality measurements made in the modified SMIRT at Station 5. Data have been averaged according to pairs of the eight zones in the wakes of the eight HX modules, which are shown in the diagram below the table. Axial airspeed and turbulence in zones 6 and 8 near the inner wall and floor are somewhat higher than average, and these same parameters are below average in zones 1 and 3 near the outer wall and ceiling.

Figures 15(a) to **(e)** present comparisons between flow parameters actually measured across Station 5 in the modified IRT [10] and those measured at the same station in the modified SMIRT. Figure 15(a) shows the vertical distribution of axial airspeed on the centerlines of each tunnel. Airspeeds have been normalized by the average airspeed across the section. In the IRT, two deficits are apparent from the two tie plates in the array of turning vanes in Corner D that were described earlier. By contrast, the data from the SMIRT, which had no tie plates, show much less flow distortion.

Figure 15(b) shows the lateral distribution of normalized axial airspeed at the mid-elevation of Station 5. Here the flows in the IRT and SMIRT are in very close agreement. The wakes of each D-corner turning vane are obvious in both, particularly near the inner wall where the vanes are relatively close to the station. The drop in airspeed that occurs in the IRT from mid-tunnel to the outer wall is modeled almost exactly in the SMIRT. At the center, the SMIRT distribution shows a deficit in airspeed attributed to the rather blunt centerbody in the model heat exchanger. The IRT distribution actually shows a rise in airspeed at the center, which is unexplained, although the HX centerbody in the IRT is much more streamlined than in the SMIRT.

Yaw flow angles across Station 5 are shown in Figure 15(c). The IRT and SMIRT distributions match very closely in the center area. The large differences near the inner wall are attributed to the fact that the IRT has a rounded inner corner where the C-D leg meets the Stilling Chamber, but the SMIRT has a square corner.

In Figure 15(d) the lateral distributions of axial turbulence intensity are shown for the IRT and SMIRT. Agreement is very good near the outer wall. The differences near the inner wall are apparently the result of less decay of the turbulence from the D-corner turning vanes in the SMIRT. Apparently, the decay distance does not scale exactly. The amount of decay may also depend on elapsed time, and SMIRT time periods are only 1/10 that of equivalent IRT periods.

Finally, Figure 15(e) illustrates the generally isotropic nature of the turbulence in both the IRT and SMIRT. Here axial turbulence intensity is plotted versus the lateral turbulence intensity occurring at the same location and time. Equality of these two parameters would represent ideal isotropic behavior.

Station 6: Mid-Length of the Test Section

Figure 16 and **Table 7** describe the flow distribution measured across Station 6, at the mid-length of the Test Section where test models are normally mounted in the IRT. It should be noted that these Test Section data were taken without the original SMIRT spraybar model, which had a very high drag and no longer represented the current streamlined spraybars in the IRT. Zero drag was determined to be a closer representation to the best flow quality attainable in the modified IRT, so no spraybar model was used. Figure 16(a) illustrates the locations of the five vertical traverses that were made with both hot-wire and 5-hole probes to obtain these data.

Figure 16(b) shows a very uniform vertical profile of the axial airspeed. Referring to Tables 2 and 6, the airspeed coefficient of variation (COV) of this profile projected for the modified IRT was only 0.2 percent, compared to a COV of 0.4 percent in the baseline IRT. When only the 4-ft x 5-ft (1.2-m x 1.5-m) core of the test section flow (Station 6′) is examined, the COV was estimated to improve from the 0.2 percent measured in the baseline IRT to a negligible 0.02 percent in the modified SMIRT. The turbulence intensity for the 4-ft x 5-ft core is reduced by the modifications from 0.6 to 0.3 percent at 350 mph. Baseline IRT turbulence data for the entire 6-ft x 9-ft (1.8-m x 2.7-m) cross-section were not available, but in the SMIRT this larger zone had a turbulence intensity of 0.4 percent. The axial airspeed COV and turbulence intensity projected for the test section in the modified IRT were so low that the mixing of the nozzle sprays normally provided by turbulence might be adversely affected. Incomplete mixing would result in a series of thin, clearly visible horizontal cloud "layers", instead of one uniform cloud throughout the IRT test section.

Figures 16(c) and (d) show the vertical variation of pitch and yaw angle graphically, while their standard deviations are listed in Table 7. The standard deviation of the pitch flow angles projected for the modified IRT was 0.3 deg, compared to 0.6 deg in the baseline IRT. When examining the center core flow area (4-ft x 5-ft), the standard deviation of pitch angle was estimated to drop from 0.6 to 0.3 deg. The standard deviations of yaw flow angles in the test section of the modified IRT were projected to be only 0.2 deg, compared to 0.7 deg measured in the baseline IRT. In the center core flow area, the standard deviation in yaw angle was projected to drop from 0.6 deg to 0.2 deg, as a result of the tunnel modifications.

Bar Chart Summary of Flow Quality Improvements

Bar charts are presented in **Figures 17(a)** to **(c)** to illustrate the estimates of the relative sizes of the improvements in flow quality parameters at three key stations in the IRT as a result of the 1999 upgrades. These charts are a graphical representation of the data in Table 1.

Lessons Learned During the SMIRT Project

1. A. substantial amount of pressure data should be taken around the model loop, including differential pressure data across all elements which can produce a loss in total pressure.
2. Both major and minor internal details should be modeled with as much accuracy as possible. In these studies, such details would include the OGVs, the tie plates in the turning vanes, the centerbody in the heat exchanger, and the inside corner fairings.
3. Unless all flow distorting elements are modeled accurately, the model results may often lead to optimistic estimates of the sizes of flow defects.
4. The method used by the heat exchanger designer to estimate drag loss was very inaccurate, for both the model and full scale HXs. The data from this study and from IRT measurements should be used to correct the method used.
5. The instrumentation and data acquisition methods used in this study were very satisfactory and are recommended for future programs.
6. The initial assumption that Reynolds number matching would not be required for accurate modeling of flow defects was verified.

Conclusions

The test program in the scale-model IRT (SMIRT) facility has accomplished its stated goals. Tests in the SMIRT provided quantitative estimates of the flow quality improvements to be expected after major modifications were made to the IRT. SMIRT tests also confirmed the absence of flow problems associated with the outlet guide vanes that condition the flow downstream of the fan, or with new expanding and contracting corner turning vanes of a novel design. These model tests allowed facility engineers to avoid costly full-scale testing of new components in the IRT and interference with the very full test schedule of the IRT. The SMIRT test procedures and results also established the basis for many of the re-activation tests in the modified IRT. The SMIRT facility can be made available for future testing of proposed IRT modifications or as an independent subsonic wind tunnel facility.

References

1. Soeder, R. H.; Sheldon, D. W.; Andracchio, C. R.; Ide, R. F.; Spera, D. A.; and Lalli, N. M.: NASA Lewis Icing Research Tunnel User Manual. NASA TM 107159, 1996.

2. Arrington, E. A.; Pickett, M. T.; Sheldon, D. W.: Flow Quality Studies of the NASA Lewis Research Center Icing Research Tunnel Circuit. NASA TM 106545, 1994.

3. Arrington, E. A.; Gonsalez, J. C.; Kee-Bowling, B. K.: Flow Quality Studies of the NASA Lewis Research Center Icing Research Tunnel Circuit (1995 Tests). NASA TM 107479, 1998.

4. Irvine, T. B., Kevdzija, S. L., Sheldon, D. W., and Spera, D. A.: Overview of the Icing and Flow Quality Improvements Program for the NASA-Glenn Icing Research Tunnel, the NASA Glenn Research Center Icing Research Tunnel, AIAA-2001-0229. NASA Glen Research Center 2001.

5. Sheldon, D. W., Andracchio, C. R., Krivanek, T. M., Spera, D. A., and Austinson, T. A.: Lessons Learned and Results from the Construction Phase and Qualification Testing of the Icing Research Tunnel Upgrades, AIAA-2001-0231. NASA-Glenn Research Center, 2001.

6. Canacci, V. A.; Gonsalez, J. C.: Flow Quality Measurements in an Aerodynamic Model of the NASA Lewis Icing Research Tunnel. AIAA-95-2389, NASA Lewis Research Center, 1995.

7. Canacci, V. A.; Gonsalez, J. C.; Spera, D. A.; and Weaver, H. L.: Scale Model Icing Research Tunnel Validation Studies. AIAA-98-0706, NASA Lewis Research Center, 1998.

8. Canacci, V. A.; Spera, D. A.; and Gonsalez, J. C.: Flow Quality Studies of the Scale Model Icing Research Tunnel and Projections to the Full-Scale Modified IRT. AIAA-99-0307, NASA Lewis Research Center, 1999.

9. Gonsalez, J. C, and Arrington, E. A.: Aerodynamic Calibration of the NASA Lewis Icing Research Tunnel (1997 Test). AIAA-98-0633, NASA Lewis Research Center, 1998.

10. Gonsalez, J. C., Arrington, E. A., and Curry, M. III: Flow Quality Surveys in the NASA Glenn Icing Research Tunnel (2000 Tests), AIAA-2001-0232. NASA Glenn Research Center, 2001.

11. Gonsalez, J. C., Arrington, E. A., and Curry, M. III: Flow Quality Surveys in the NASA Glenn Icing Research Tunnel (2000 Tests), AIAA-2001-0232. NASA Glenn Research Center, 2001.11.

12. Anon.: Installation and Operation Manual for Model 666N, NX, P Air Turbine Motor. TM 89-109, Tech Development Inc., 1989.

13. Cloudy and Britton, Inc.: NASA IRT Heat Exchanger Data Tables for Performance Curves, Appendix A, Phase 2 Special Study Report 2. Aero Systems Engineering, 1996.

14. Olsen, W.; Van Fossen, J.; and Nussle, R: Measured Performance of the Heat Exchanger in the NASA Icing Research Tunnel Under Severe Icing and Dry Air Conditions. NASA TM 100116, 1987.

15. Anon.: Model DAP IFA Thermal Anemometry Software Package Instruction Manual, Revision A. TSI, Inc., 1993.

16. DeArmon, J. D.: PACS User Manual for Probe Actuator Control System. NASA Lewis Research Center (unpublished), 1993.

Table 1
Comparison of Flow Quality Parameters Measured in the SMIRT and IRT

Tunnel station and Flow parameter	IRT Before modification	IRT after modification	SMIRT after modification	
			Long Baffles	Short baffles
2. Vent Tower				
Airspeed COV (%)	36.6	26.2	13.9	26.3
Axial turbulence intensity (%)	23.4	22.7	21.5	21.1
Lateral turbulence intensity (%)	19.2	21.5	16.0	16.3
Pitch angle STD (deg)	6.4	2.7	2.7	2.0
Yaw angle STD (%)	5.3	1.9	1.7	2.3
5. Spraybar inlet				
Airspeed COV (%)	21.5	4.2	5.2	4.5
Axial turbulence intensity (%)	8.4	2.6	3.7	3.8
Lateral turbulence intensity (%)	6.3	3.2	3.8	3.2
Pitch angle STD (deg)	1.0	1.4	0.8	1.0
Yaw angle STD (%)	3.5	2.4	1.4	1.3
6. Test Mid-Section: 6-ft x 9-ft zone			No spraybars	
Airspeed COV (%)	0.4	0.4	0.2	---
Axial turbulence intensity (%)	---	---	0.4	---
Lateral turbulence intensity (%)	---	---	---	---
Pitch angle STD (deg)	0.7	0.7	0.3	---
Yaw angle STD (%)	0.7	0.3	0.2	---
6'. Test Mid-Section: 4-ft x 5-ft zone			No spraybars	---
Airspeed COV (%)	0.2	0.3	0.02	---
Axial turbulence intensity (%)	0.6	0.6	0.3	---
Lateral turbulence intensity (%)	---	0.8	0.3	---
Pitch angle STD (deg)	0.7	0.5	0.3	---
Yaw angle STD (%)	0.5	0.3	0.2	---

Table 2
Summary of Flow Quality Parameters Averaged Across Station 2:
Vent Tower Section Between Fan and Corner C

Configuration of fan nacelle baffles	Variation of axial airspeed, *COV* (percent)	Turbulence intensity, *DU/U* (percent)	STD of pitch flow angle $d\alpha$ (deg)	STD of yaw flow angle, $d\beta$ (deg)
IRT and SMIRT in Baseline (Original) Circuit Configuration (a)				
IRT: No OGVs	36.6	23.4	6.4	5.3
SMIRT: No OGPs	32.4	27.6	6.8	6.8
SMIRT in Modified Circuit Configuration (b) Two Lengths of Radial Outlet Guide Plates (OGPs) Simulating OGVs				
No OGPs	41.3	33.5	5.1	5.5
5 OGPs with $L = 0.6\ D$	26.3	21.2	2.0	2.3
Least swirl: $L = 1.0\ D$	19.1	19.0	1.7	1.5
5 OGPs with $L = 1.4\ D$ (c)	**13.9**	**21.5**	**2.7**	**1.7**

(a) W-shaped HX; no OGVs
(b) Expanded-width C-D leg, with flat heat exchangers
(c) Estimate for IRT; expected to be closest to final configuration of modifications

Table 3.
Summary of Changes in Average Flow Quality Parameters
Estimated from SMIRT Test Data for IRT Stations

Station no.	Section Name	Variation in axial airspeed, *COV* (percent)		Axial turbulence intensity, *u'/U* (percent)		STD of pitch flow angle, $d\alpha$ (deg)		STD of yaw flow angle, $d\beta$ (deg)	
		Actual: Baseline IRT	**Est.: Modified IRT**	Actual: Baseline IRT	**Est.: Modified IRT**	Actual: Baseline IRT	**Est.: Modified IRT**	Actual: Baseline IRT	**Est.: Modified IRT**
2	Vent tower: C-corner inlet	36.6	**13.9**	23.4	**21.5**	6.4	**2.7**	5.3	**1.7**
3	HX inlet	26.0	**14.1**	15.4	**18.8**	4.8	**1.9**	2.0	**4.6**
4	HX outlet	44.5	**7.0**	29.0	**9.0**	5.1	**0.6**	3.6	**0.6**
5	Stilling chamber: Spraybar inlet	21.5	**5.2**	8.4	**3.7**	1.0	**0.8**	3.5	**1.4**
6 (a)	Test mid-section: 6-ft x 9-ft zone	0.4	**0.2**	---	**0.4**	0.7	**0.3**	0.7	**0.2**
6' (a)	Test mid-section 4-ft x 5-ft zone	0.2	**0.02**	0.6	**0.3**	0.7	**0.3**	0.5	**0.2**

(a) Estimates without effects of spraybars; no spraybar model in SMIRT

Table 4.
Estimated Flow Quality Parameters at Station 3 in Modified IRT:
Heat Exchanger Inlet, Averaged According to HX Module Locations

Heat exchanger And Module number	Normalized axial airspeed, *U/Umean*	Variation of axial airspeed *COV* (percent)	Turbulence intensity (a) *dU/U* (percent)	STD of pitch flow angle, $d\alpha$ (deg)	STD of yaw flow angle, $d\beta$ (deg)
Outer HX					
2 (top)	0.93	13.4	20.4	2.2	4.2
4	1.02	11.9	19.0	0.5	4.5
6	1.13	15.0	20.0	1.2	4.5
8 (bottom)	1.11	16.4	21.3	0.9	4.9
Outer HX averages	1.05	16.3	20.2	1.3	4.5
Inner HX					
1 (top)	0.86	5.1	17.3	1.4	2.7
3	0.99	8.1	17.2	1.4	2.9
5	1.00	8.4	17.2	1.4	4.5
7 (bottom)	0.95	7.6	17.1	1.2	6.0
Inner HX averages	0.95	9.3	17.2	1.4	4.3
Estimated averages for Station 3	**1.00**	**14.1**	**18.8**	**1.9**	**4.6**

(a) Projected axially to scaled locations of upstream faces of IRT heat exchangers

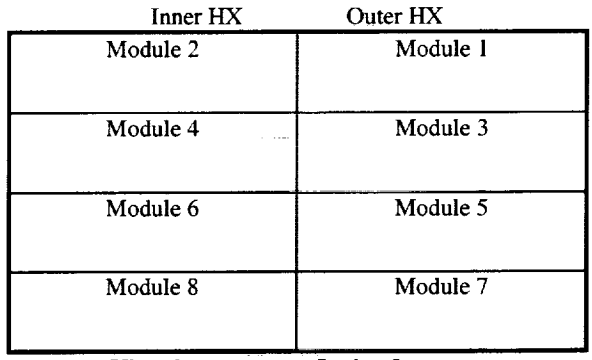

View downstream at Station 3

Table 5.
Estimated Flow Quality Parameters at Station 4 in Modified IRT:
Heat Exchanger Outlet, Averaged According to HX Module Locations

Heat exchanger And Module number	Normalized axial airspeed, *U/Umean*	Variation of Axial airspeed *COV* (percent)	Turbulence intensity, *dU/U* (percent)	STD of pitch flow angle, $d\alpha$ (deg)	STD of yaw flow angle, $d\beta$ (deg)
SMIRT Outer HX Wakes As Measured (a)					
1 (top)	0.93	8.5	10.6	---	1.1
3	0.94	7.2	10.2	---	1.2
5	0.96	7.5	10.1	---	1.4
7 (bottom)	0.97	6.8	10.4	---	1.3
SMIRT Outer HX averages as measured	0.95	7.5	10.3	---	1.2
IRT Estimates from SMIRT Measurements					
IRT outer HX wake Averages	1.05	5.8	9.0	0.6	0.6
IRTinner HX wake averages	0.95	5.8	9.0	0.6	0.6
Estimated averages for Station 4	**1.00**	**7.0**	**9.0**	**0.6**	**0.6**

(a) No measurements in wakes of Inner HX

Inner HX Wakes	Outer HX Wakes
Module 2	Module 1
Module 4	Module 3
Module 6	Module 5
Module 8	Module 7

View downstream at Station 4

Table 6.
Estimated Flow Quality Parameters at Station 5 in Modified IRT:
Spray Bar Inlet Plane, Averaged According to Pairs of HX Module Locations

Heat exchanger And Module number	Normalized axial airspeed, *U/Umean*	Variation of axial airspeed *COV* (percent)	Turbulence intensity *dU/U* (percent)	STD of pitch flow angle, $d\alpha$ (deg)	STD of yaw flow angle, $d\beta$ (deg)
Outer HX					
1 and 3 (top)	0.99	2.9	4.8	0.3	0.3
5 and 7 (bottom)	1.04	3.8	4.6	0.4	0.9
Outer HX averages	1.02	4.1	4.7	0.5	1.0
Inner HX					
2 and 4 (top)	0.98	3.2	2.6	0.1	0.1
6 and 8 (bottom)	0.99	3.5	2.5	0.2	0.6
Inner HX averages	0.98	4.0	2.6	0.3	0.6
Estimated averages for Station 5	**1.00**	**5.2**	**3.7**	**0.8**	**1.4**

Inner HX	Outer HX
Module 2	Module 1
Module 4	Module 3
Module 6	Module 5
Module 8	Module 7

View downstream at Station 5

Table 7.
Summary of Estimates of Flow Quality Parameters at Station 6 in Modified IRT:
Mid-Length of Test Section, Averaged According to Two Zones and Without Spray Bar Model

Zone	Normalized axial airspeed, *U/Umean*	Variation of axial airspeed, *COV* (percent)	Turbulence intensity, *dU/U* (percent)	STD of pitch flow angle, $d\alpha$ (deg)	STD of yaw flow angle, $d\beta$ (deg)
"6-ft x 9-ft" zone	**1.00**	**0.2**	**0.4**	**0.3**	**0.2**
"4-ft x 5-ft" zone	**1.00**	**0.02**	**0.3**	**0.3**	**0.2**

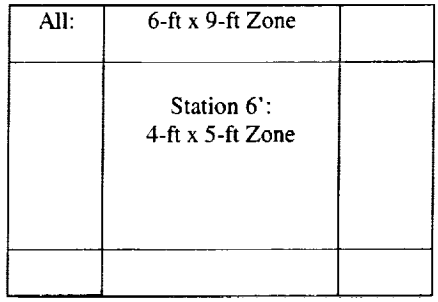

View Downstream at Station

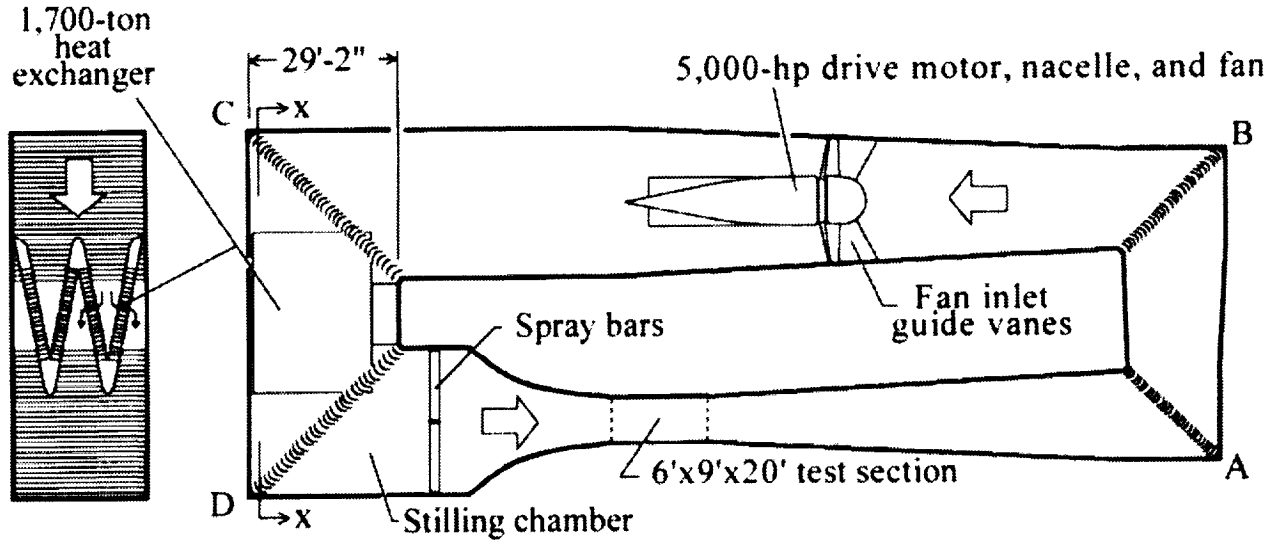

Figure 1. Current (baseline) loop configuration of the 6'x 9' Icing Research Tunnel (IRT).

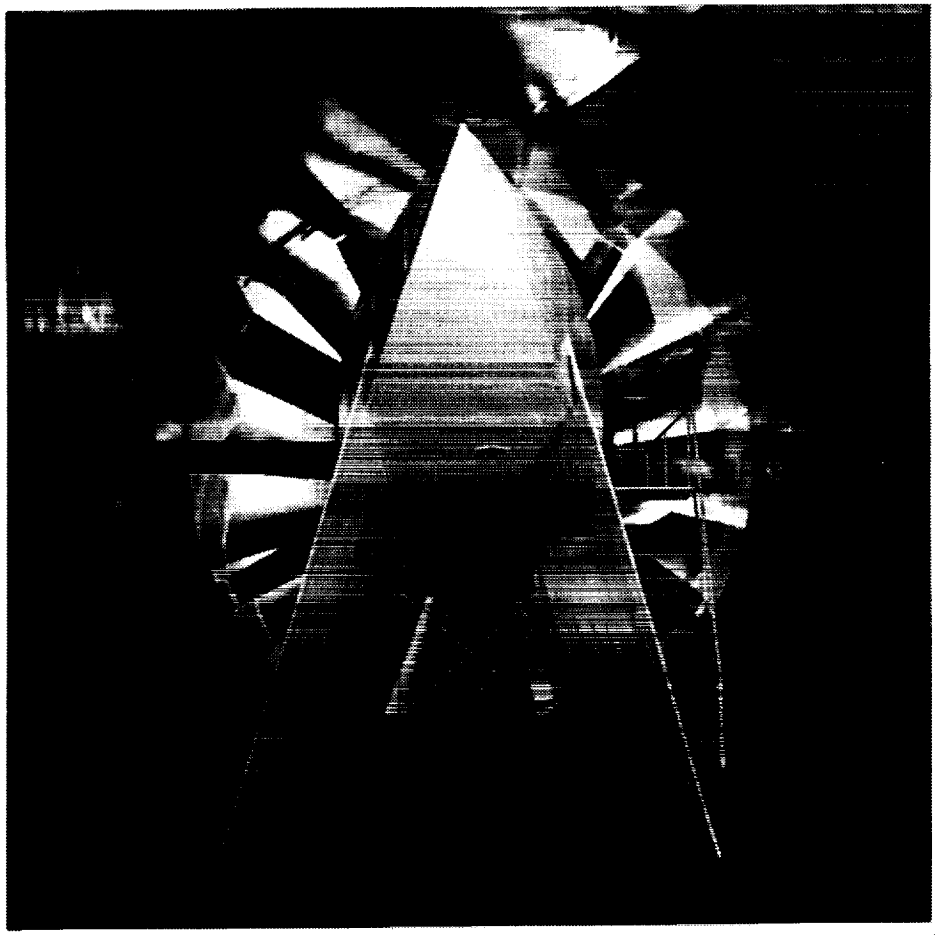

Figure 2. View upstream of IRT fan and motor housing. The two long fairings over the legs of the motor support platform are theorized to cause large variations in downstream air velocities.

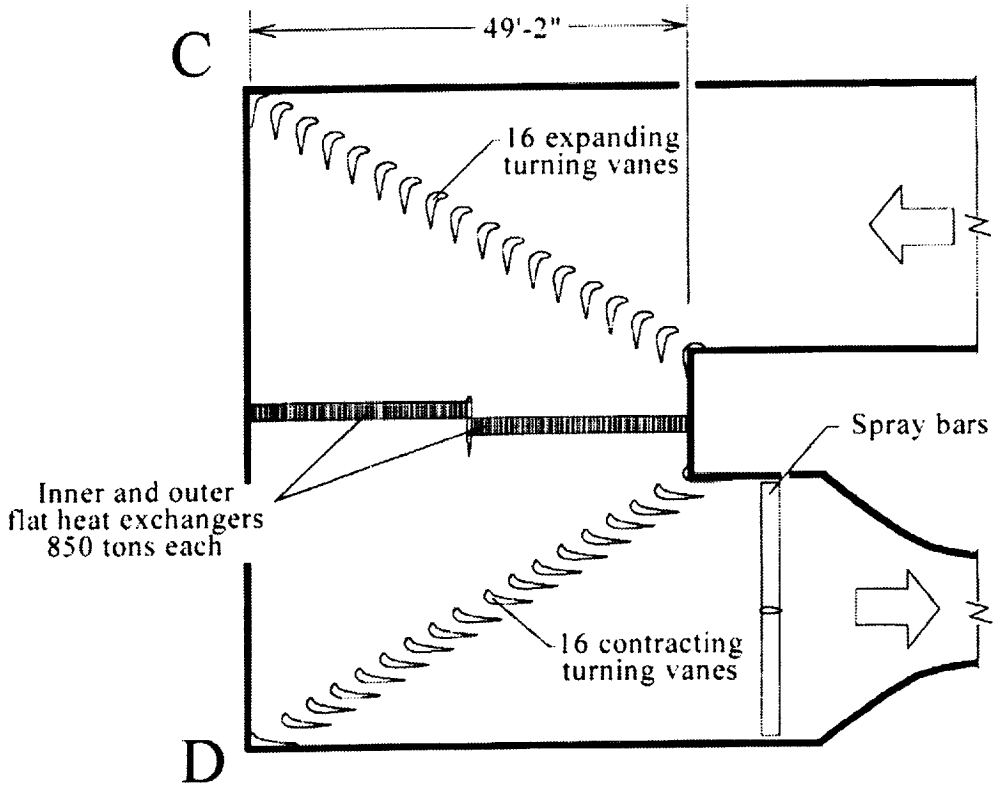

Figure 3. Planned modifications to the C-D leg of the IRT. Width is increased 68% to accommodate two flat heat exchangers. New turning vanes provide flow expansion and contraction.

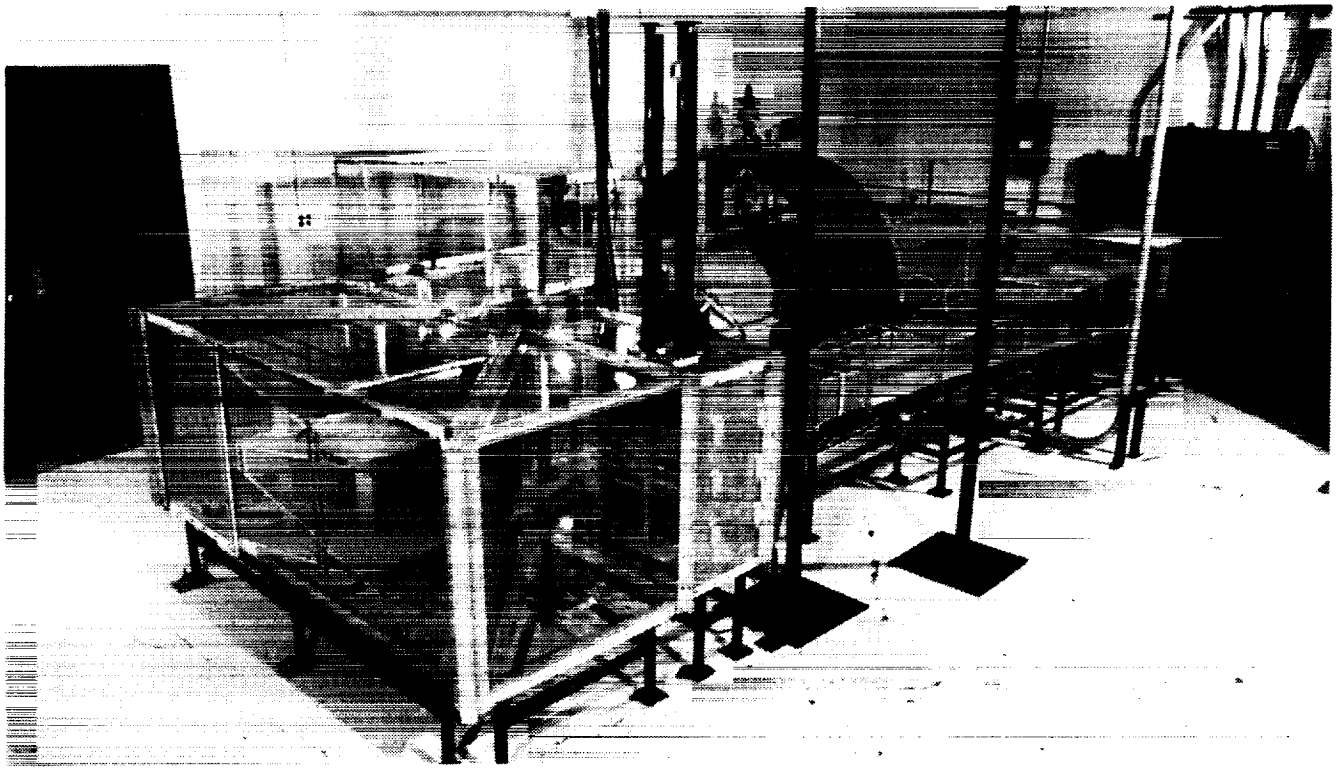

(a) General view, with baseline configuration of the C-D leg.

Figure 4. The 1/10th scale model of the IRT (SMIRT), showing two configurations of the C-D leg.

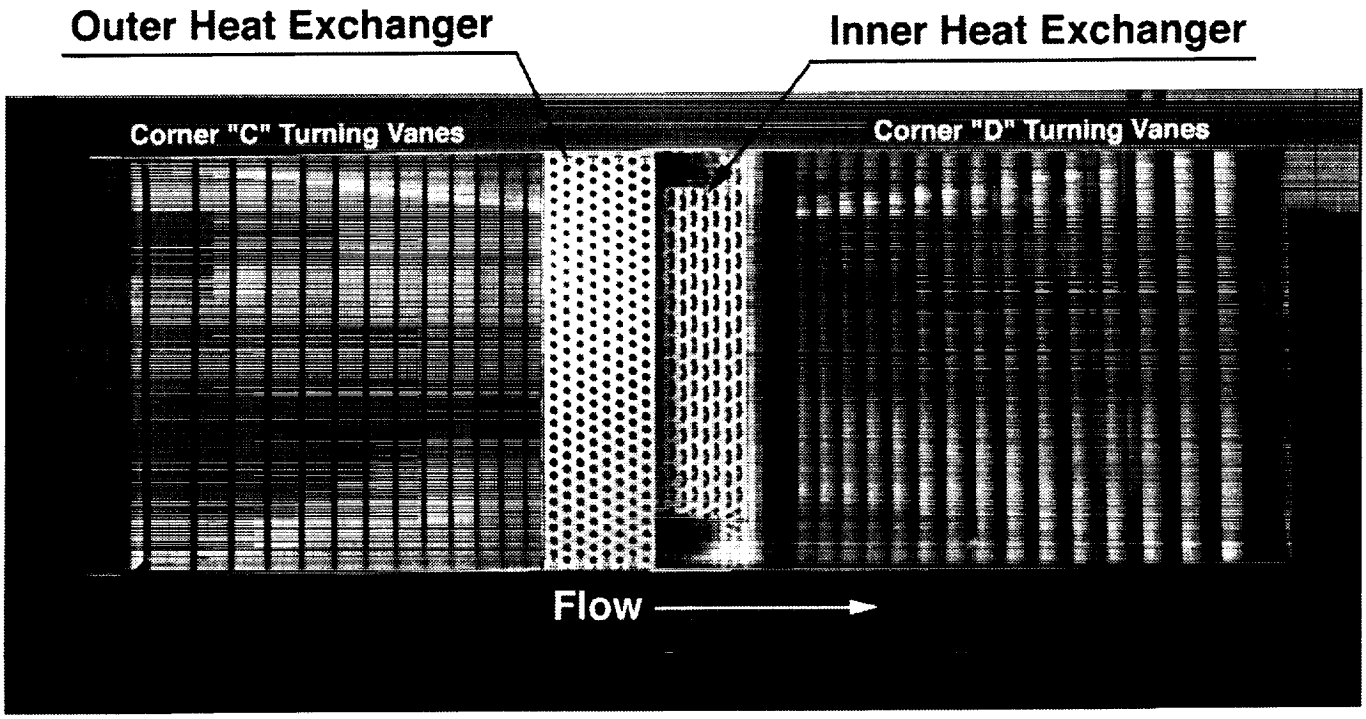

Figure 4 (b). Elevation view of the modified C-D leg. End wall is removed to show (l. to r.) the Corner C turning vanes, outer and inner heat exchangers, and Corner D turning vanes.

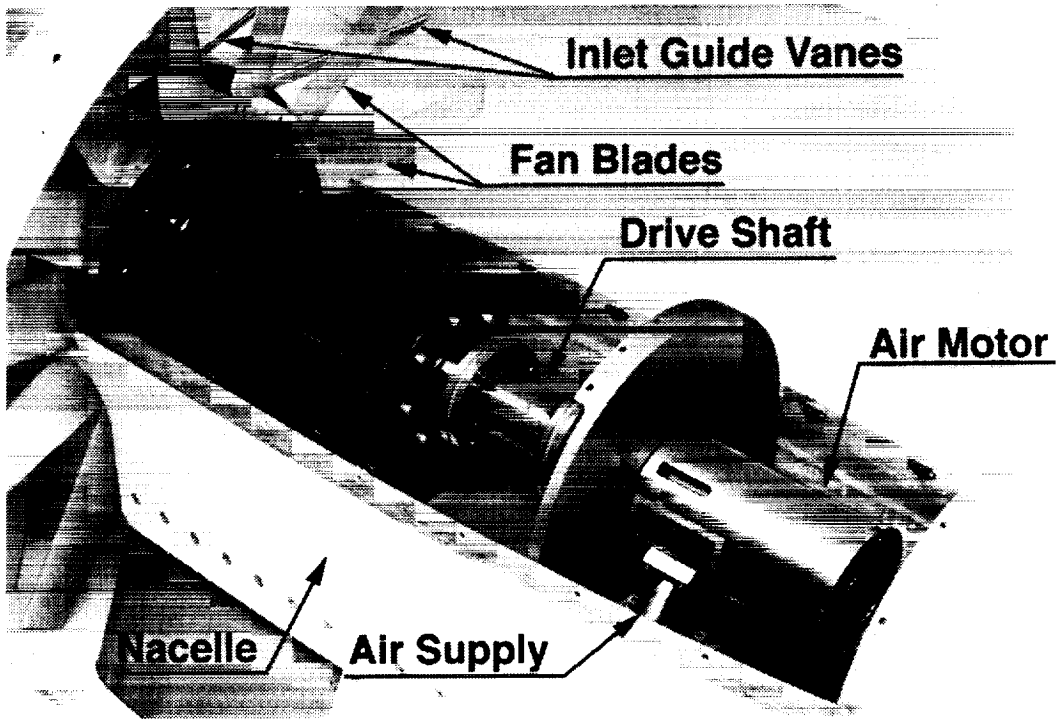

Figure 4 (c). SMIRT Fan Drive. Motor nacelle cover is removed to show the air turbine and drive shaft.

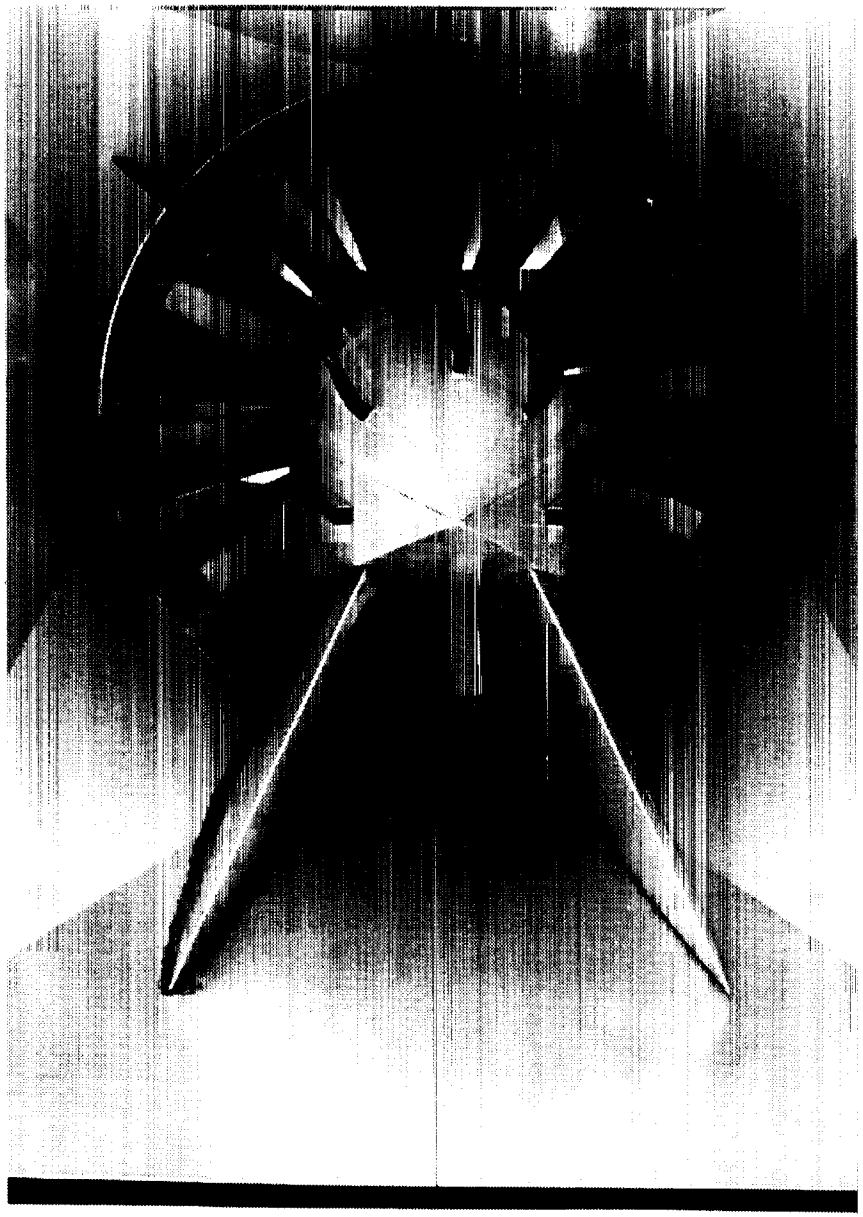

(d) Shorter OGP's, 0.6 fan diameters in length.

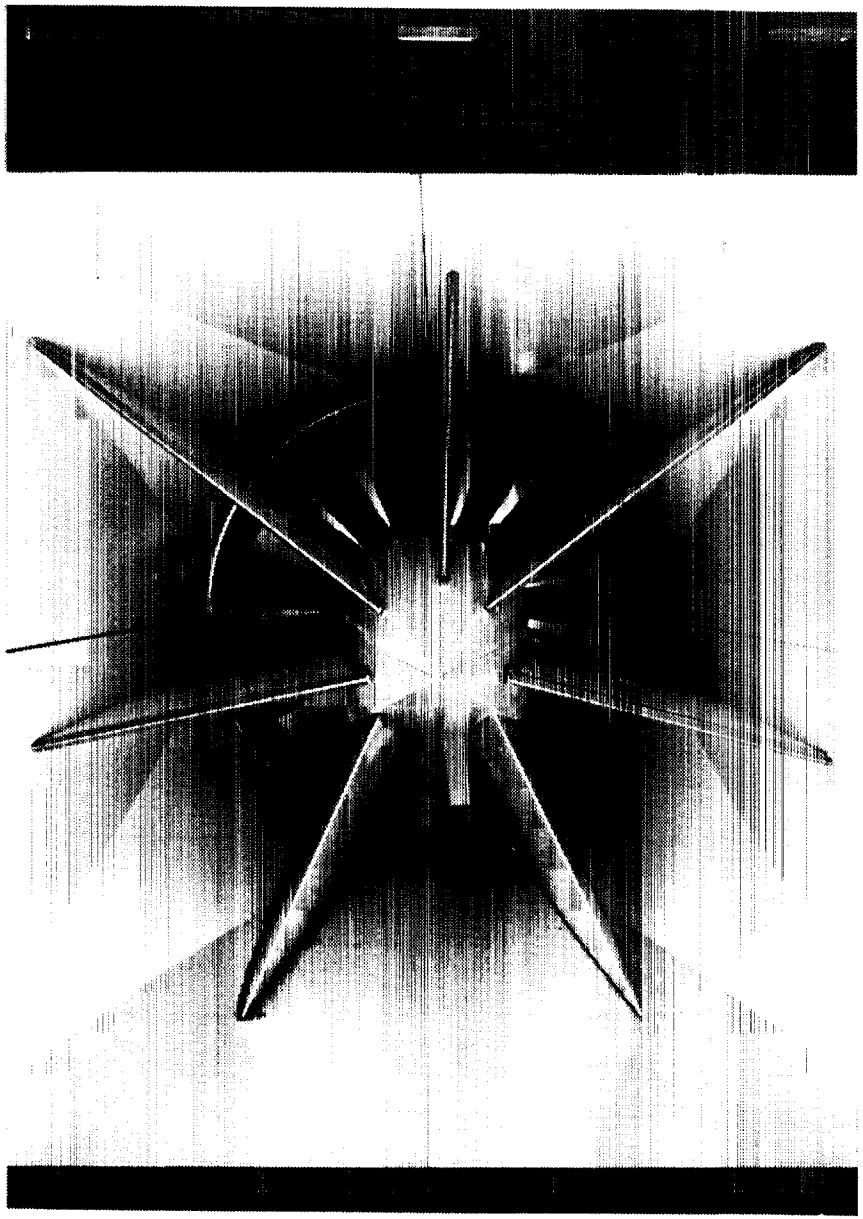

(e) Longer OGP's, 1.4 fan diameters in length.

Figure 4 (continued). Upstream view of the SMIRT fan drive with five outlet guide plates installed to simulate the IRT fan outlet guide vanes (OGV's).

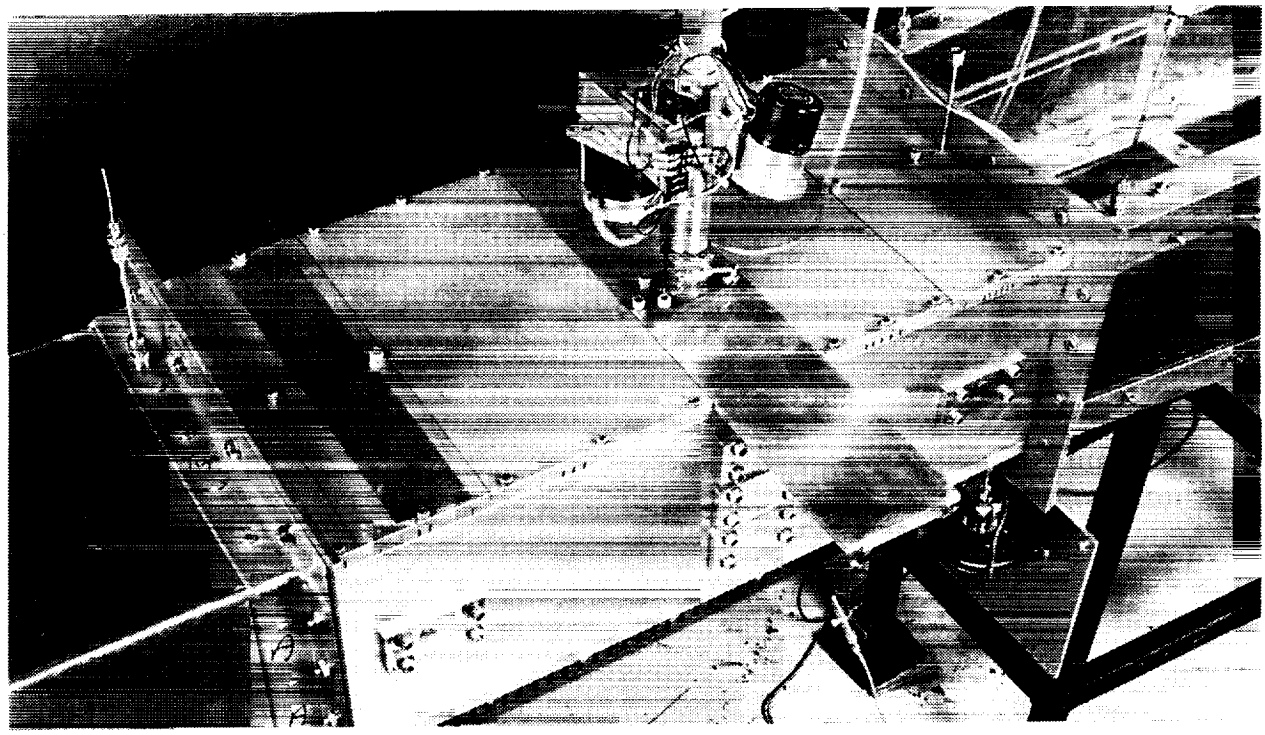

Figure 4 (f). SMIRT Test Section illustrating sliding probe actuator mounting system that maintains probe alignment when repositioning probe at various stations.

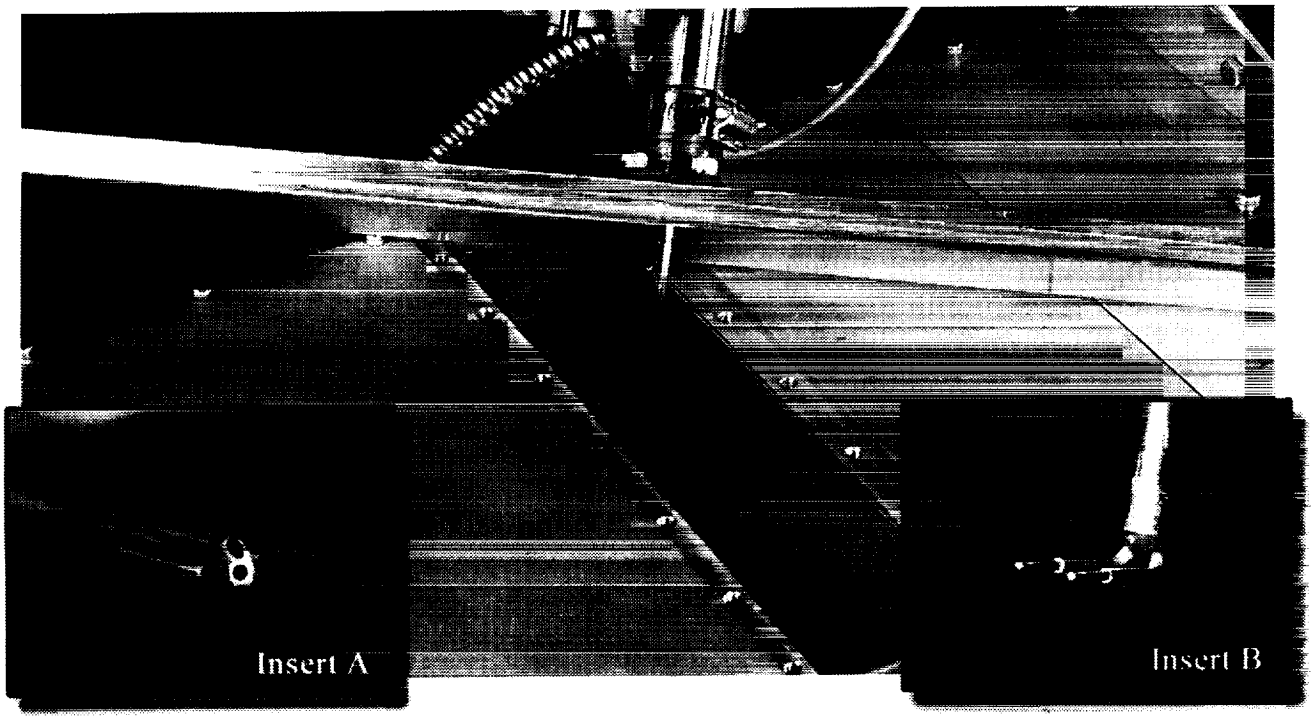

Figure 4 (g). Test Section sliding probe actuator mounting system removed.
Insert A) Five-Hole Probe
Insert B) Hot-Wire Probe

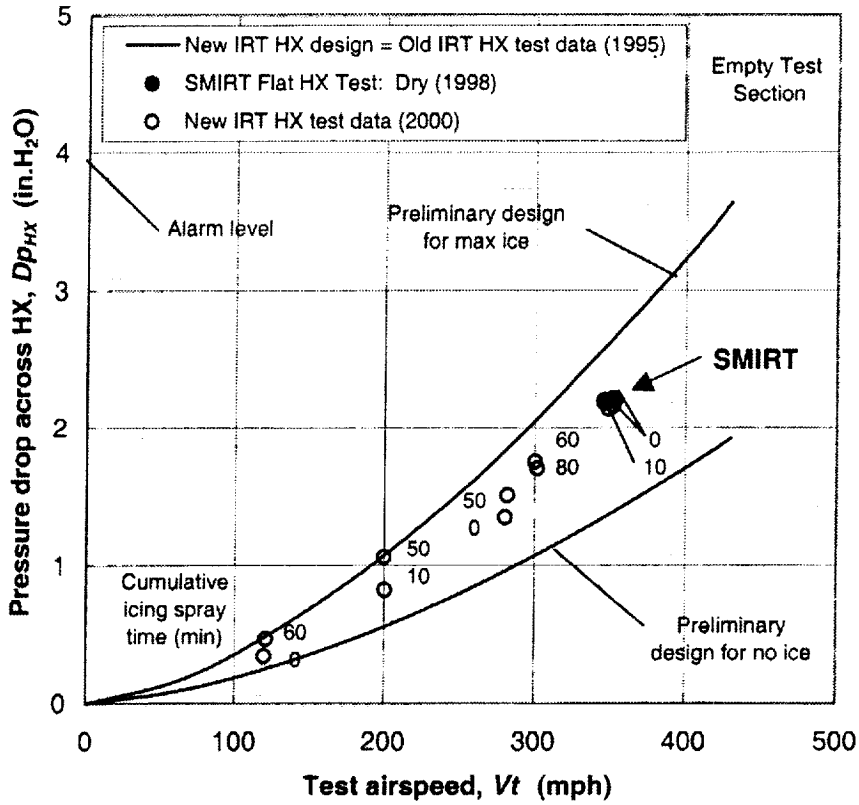

Figure 5. Pressure Drop Across IRT and SMIRT Heat Exchangers.

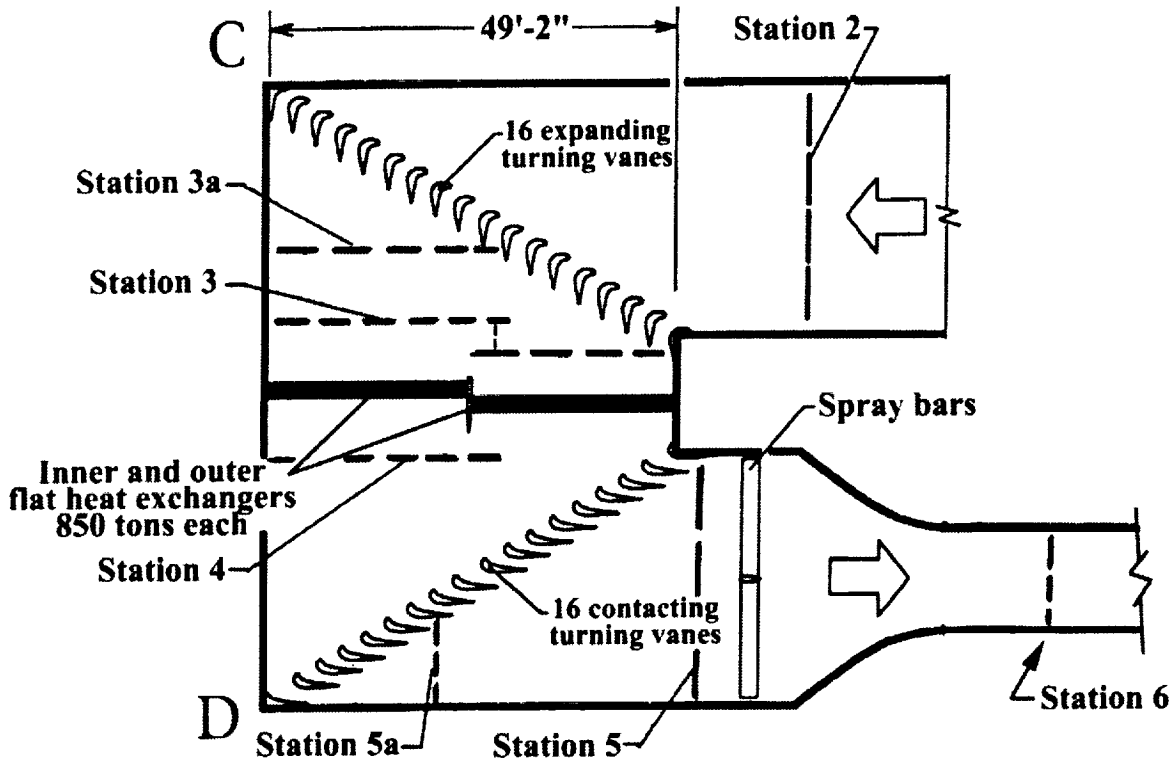

Figure 6. Stations for SMIRT Flow Quality Measurements.

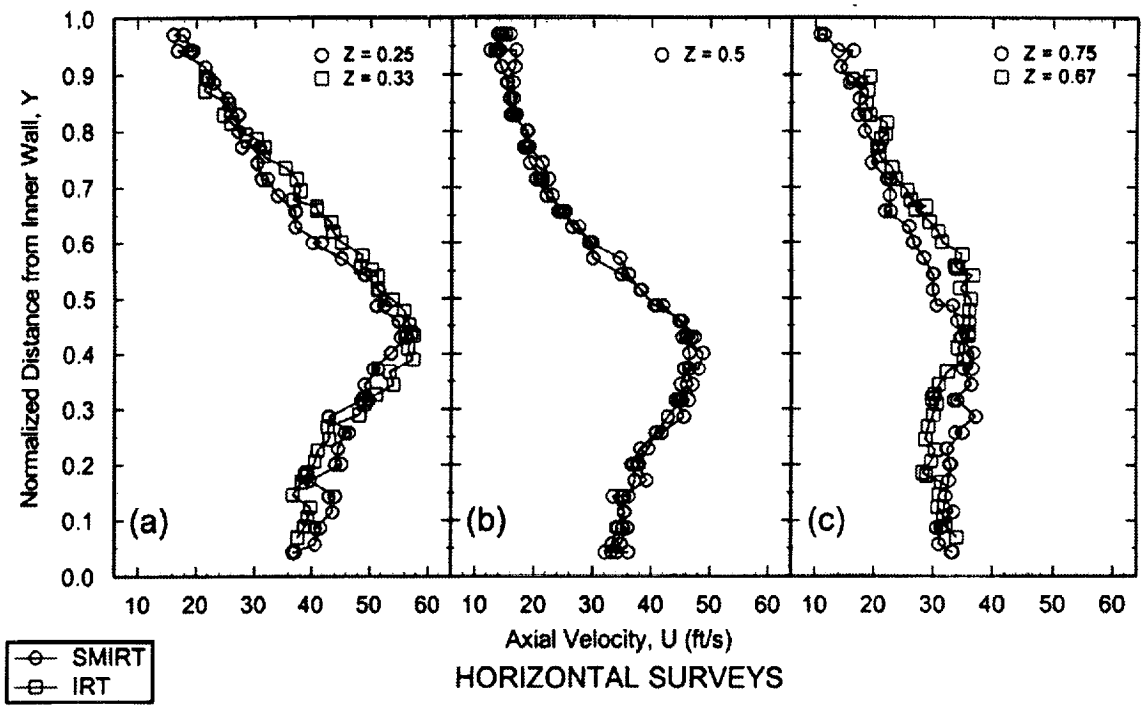

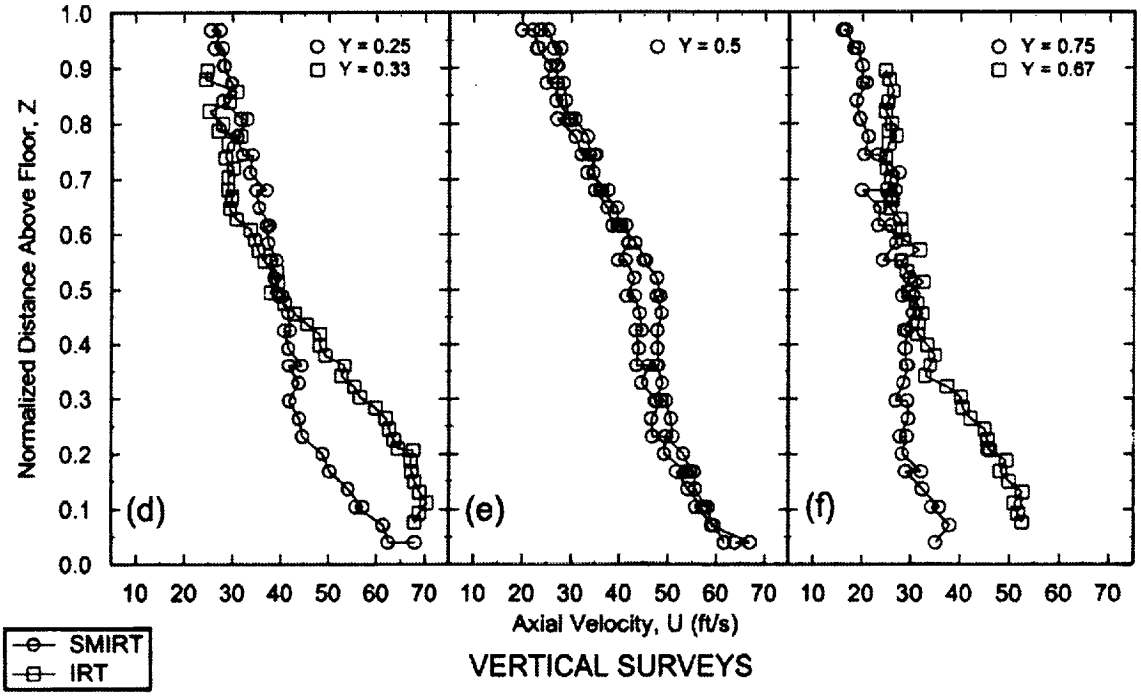

Figure 7. Comparison of unmodified SMIRT and unmodified IRT: Cartesian graphs of axial velocity across Station 2 in Vent Tower section.

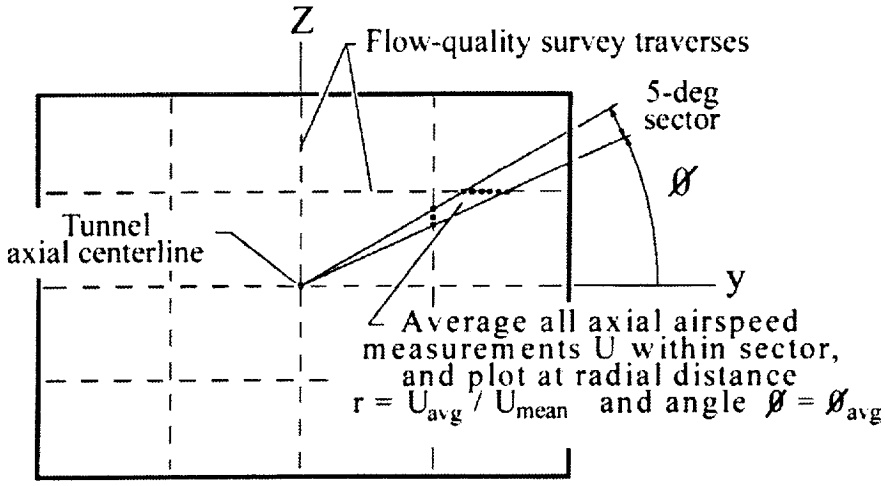

(a) Schematic diagram illustrating the method used for creating polar plots.

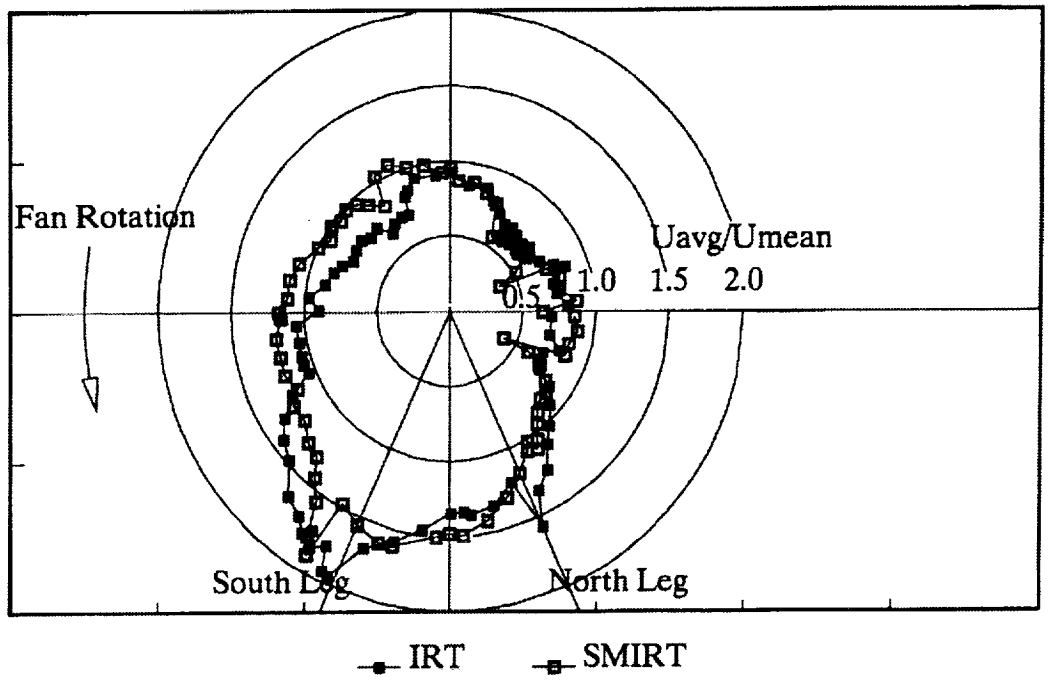

(b) Polar plot of SMIRT and IRT axial velocity ratios; view is downstream.

Figure 8. Comparison of unmodified SMIRT and unmodified IRT: Polar distributions of axial velocity ratios across Station 2 in Vent Tower section.

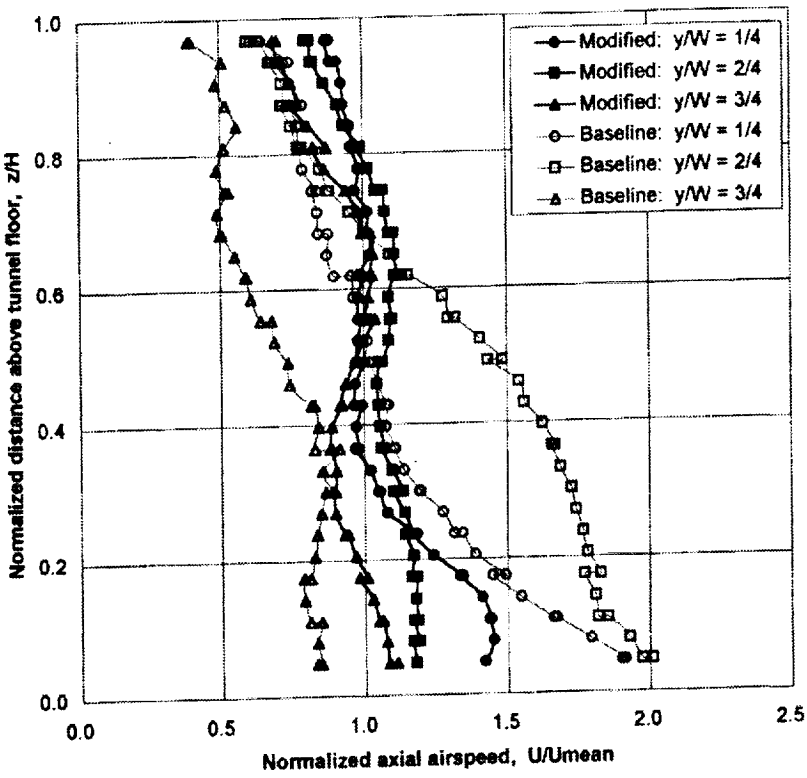

(a) Vertical distributions of axial airspeed.

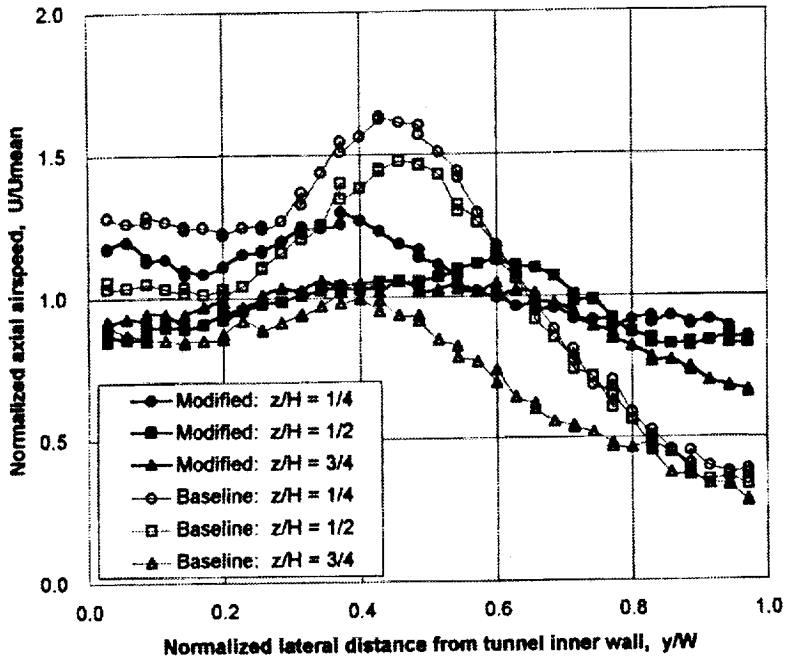

(b) Horizontal distributions of axial airspeed.

Figure 9. **Comparison of flow distribution across Station 2 (Vent Tower section) in the unmodified and modified SMIRT configurations.**

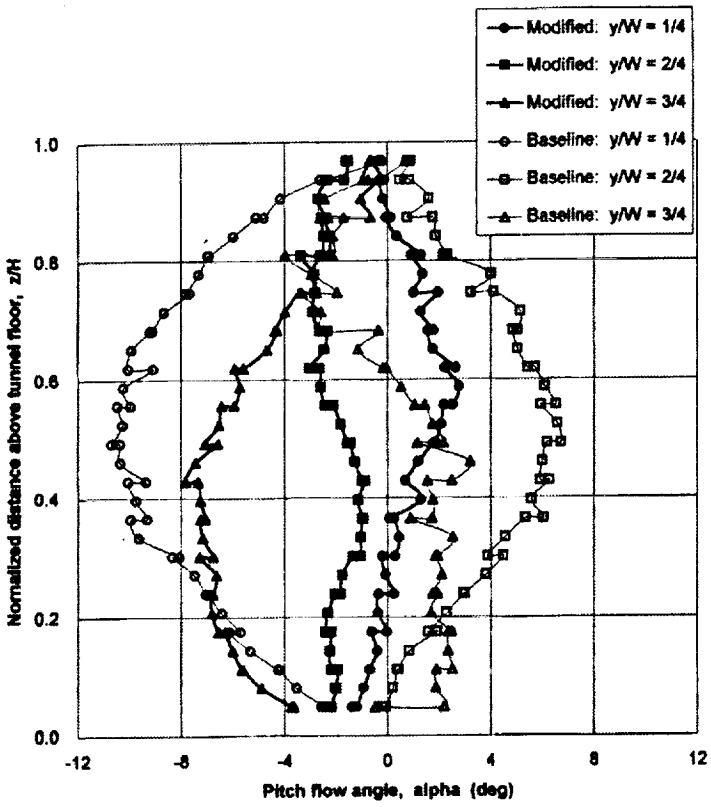

(c) Vertical distributions of pitch flow angle.

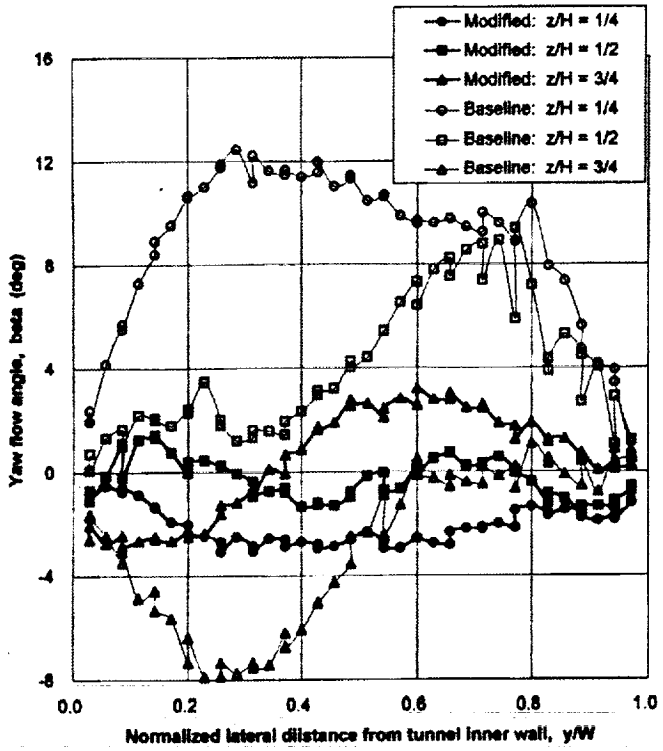

(d) Horizontal distributions of yaw flow angle.

Figure 9. Comparison of flow distribution across Station 2 (Vent Tower section) in the unmodified and modified SMIRT configurations (Concluded).

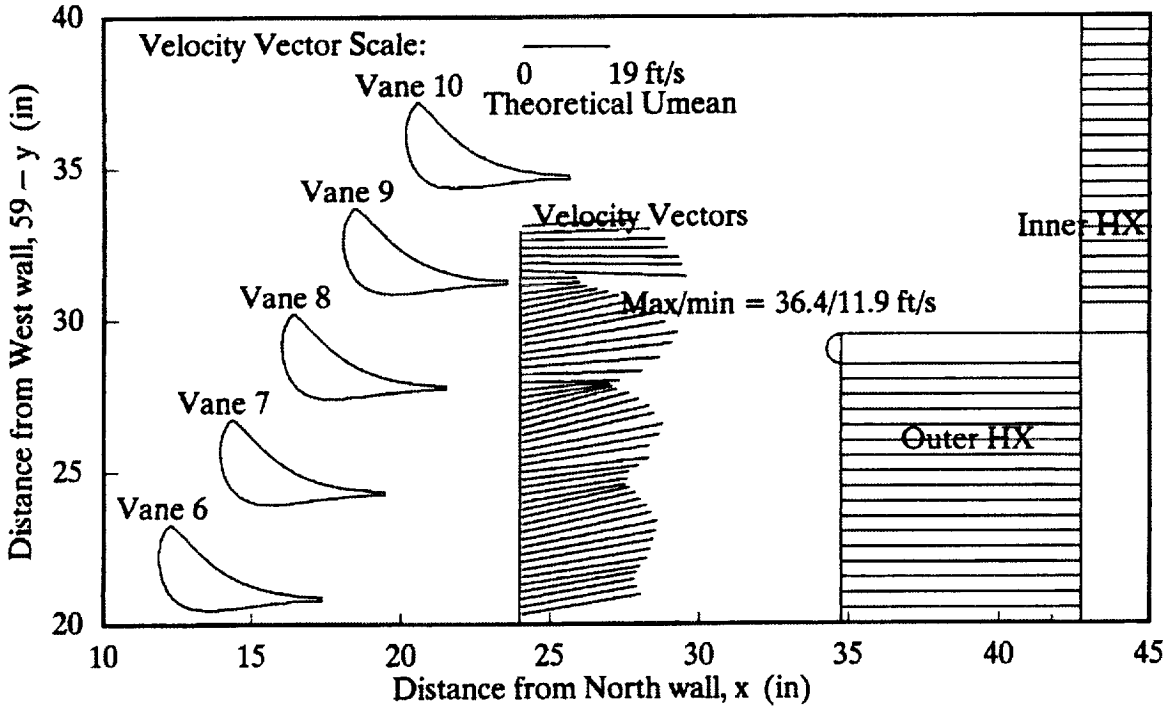

Figure 10 (a). **Flow vectors in modified SMIRT downstream of Corner C turning vanes (Station 3a).**

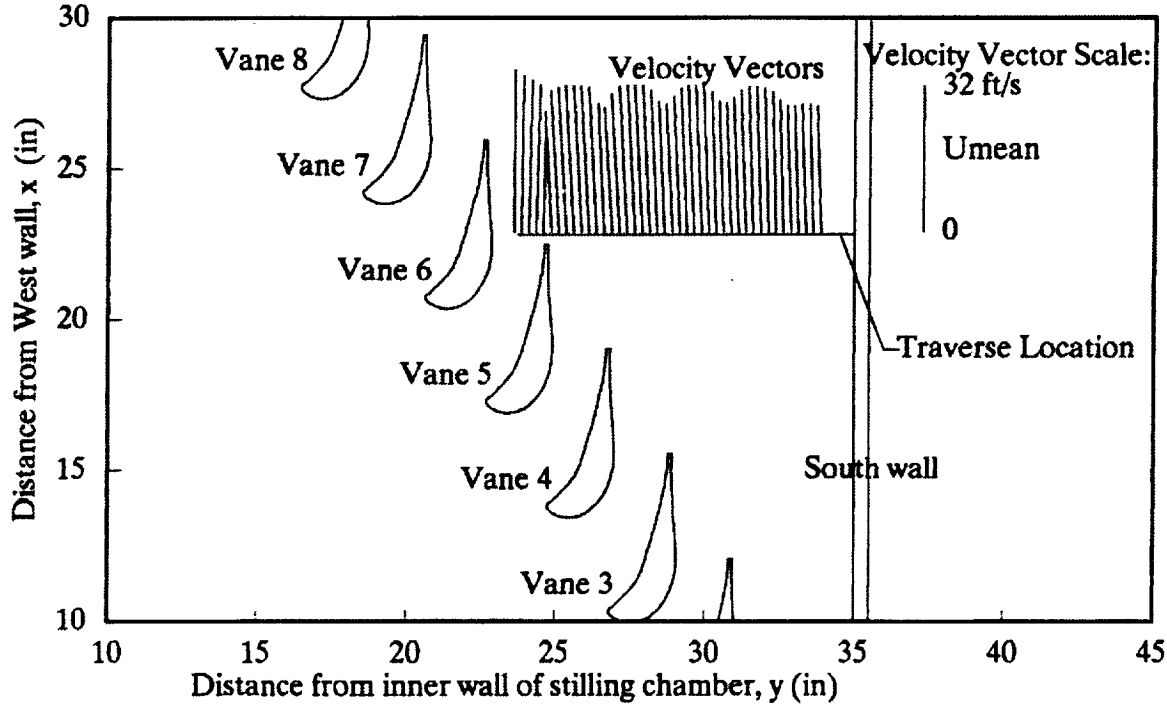

Figure 10 (b). **Flow vectors in modified SMIRT downstream of Corner D turning vanes (Station 5a).**

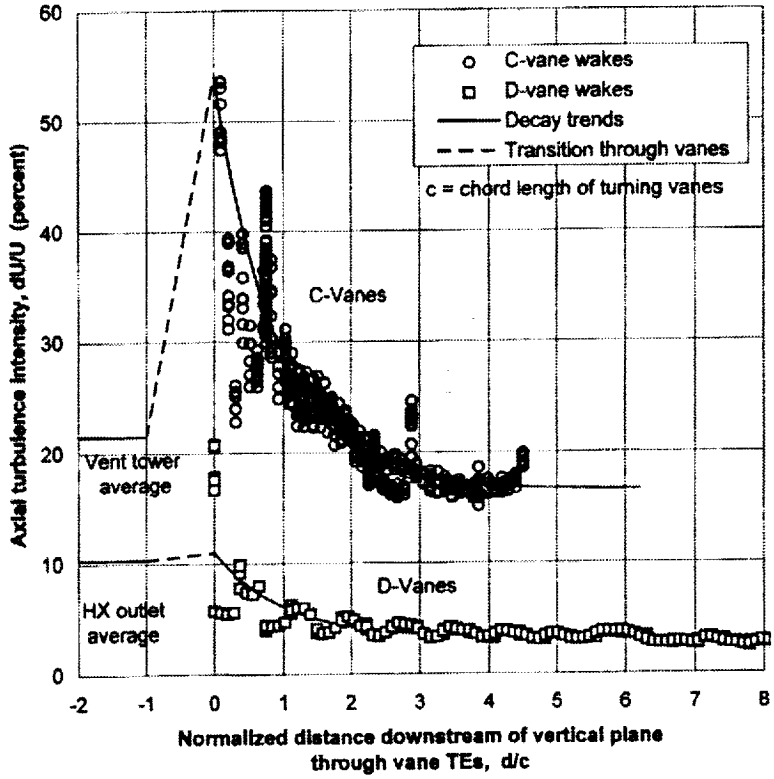

Figure 11. Changes in axial turbulence intensity with distance from trailing edge plane of corner turning vanes as measured in the modified SMIRT.

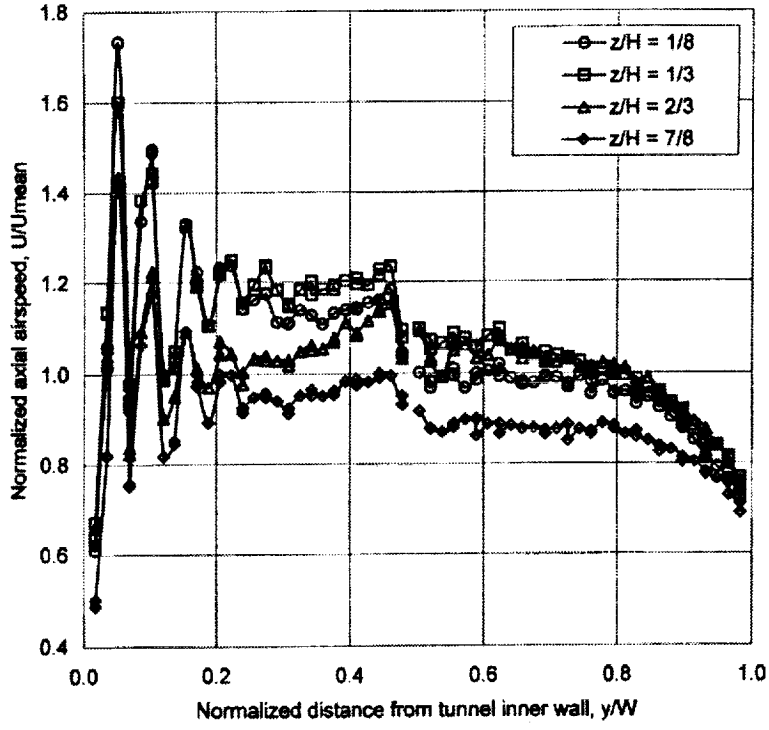

Figure 12 (a). Lateral distribution of axial airspeed in the modified SMIRT across Station 3: Heat Exchanger inlet.

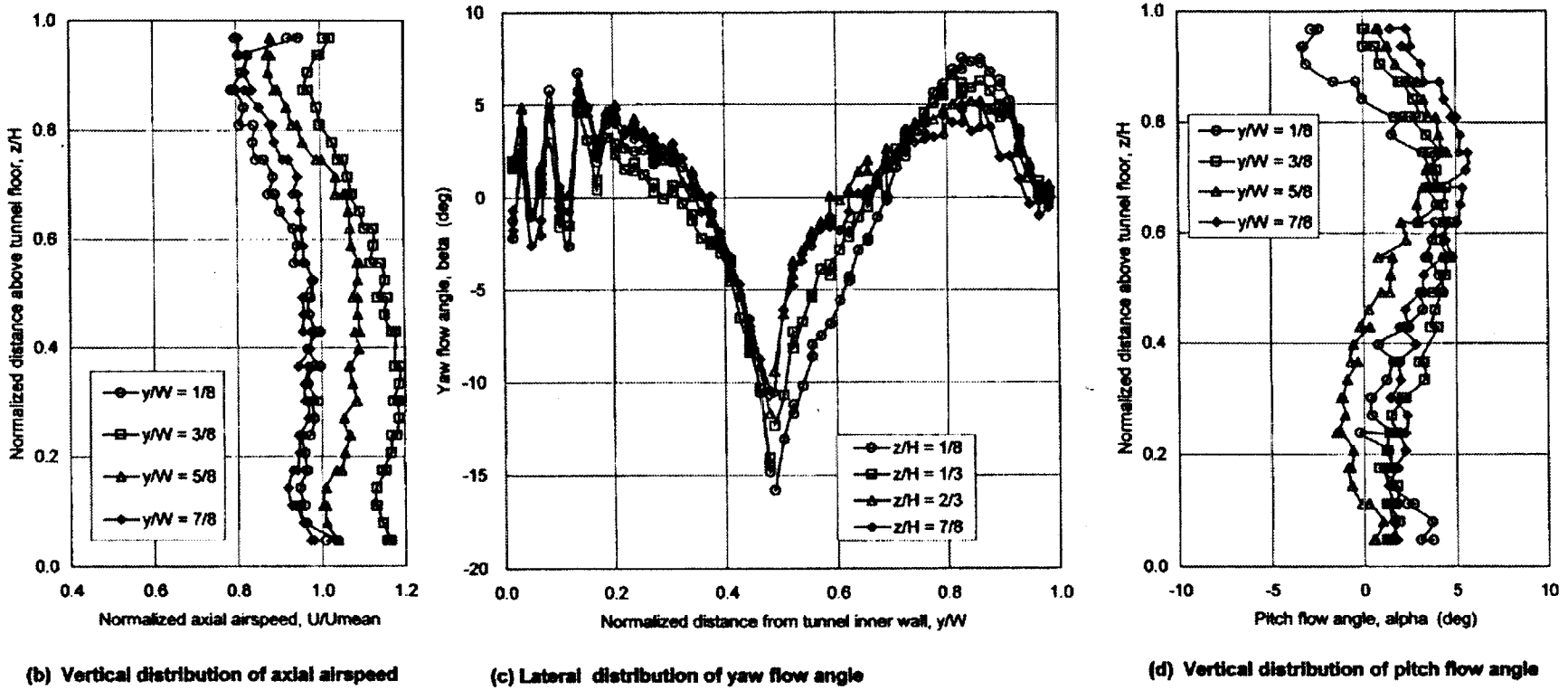

(b) Vertical distribution of axial airspeed

(c) Lateral distribution of yaw flow angle

(d) Vertical distribution of pitch flow angle

Figure 12. Flow distribution across Station 3: Heat Exchanger inlet.

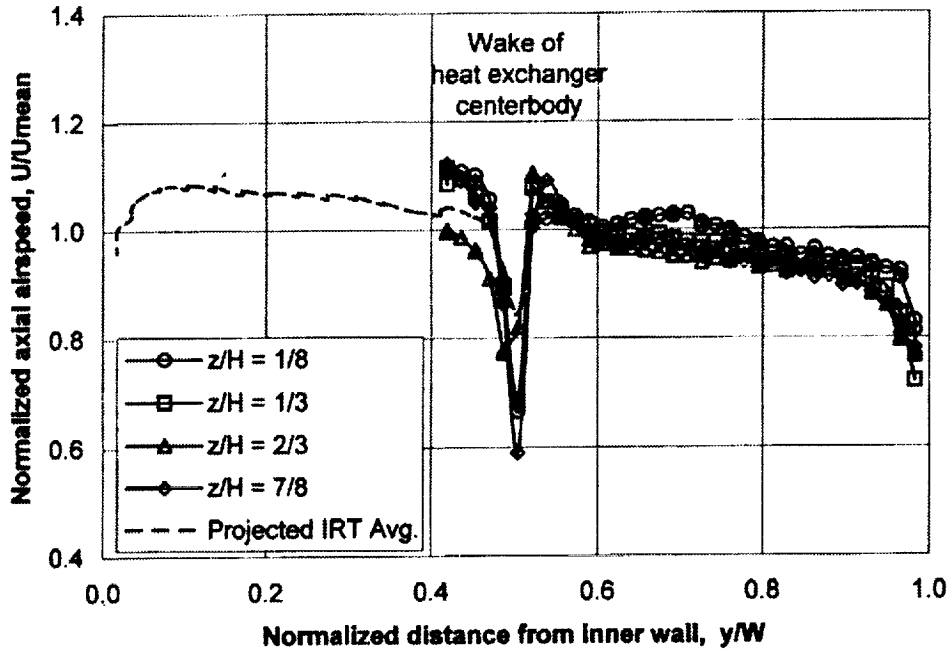

(a) Lateral distribution of axial airspeed.

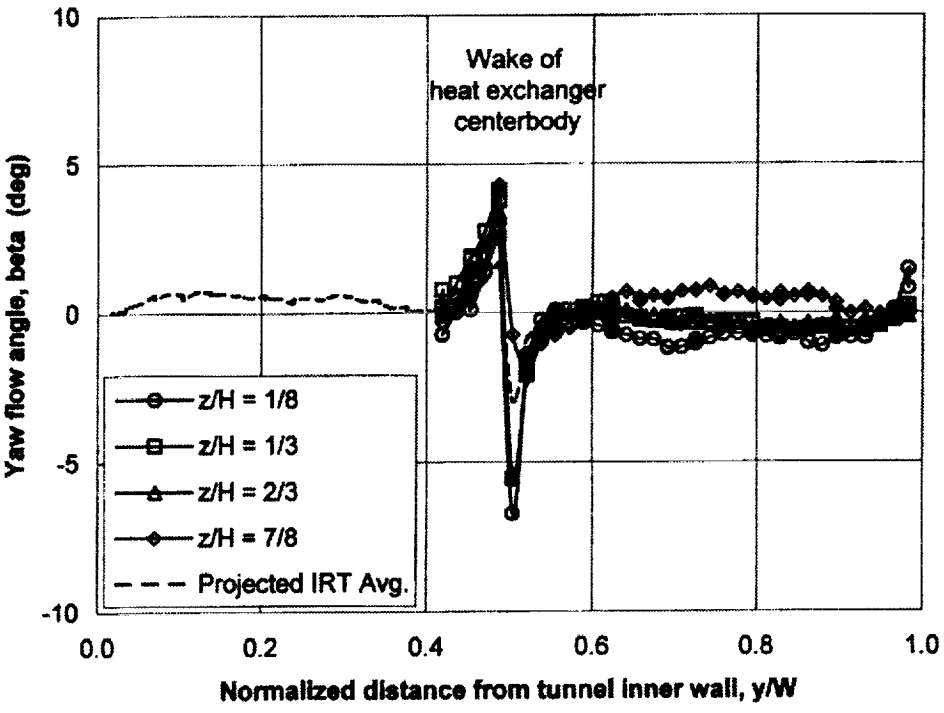

(b) Lateral distribution of yaw flow angle.

Figure 13. Flow distribution in the modified SMIRT across Station 4: Heat Exchanger Outlet.

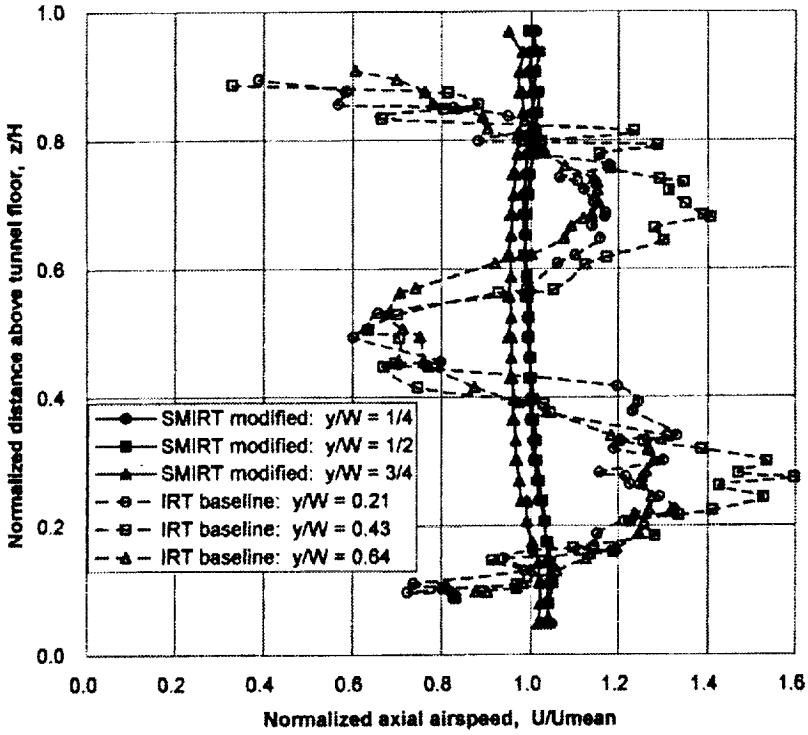

Figure 14 (a). Comparison of modified SMIRT and baseline IRT vertical axial airspeed distributions at Station 5: Spray Bar entrance plane.

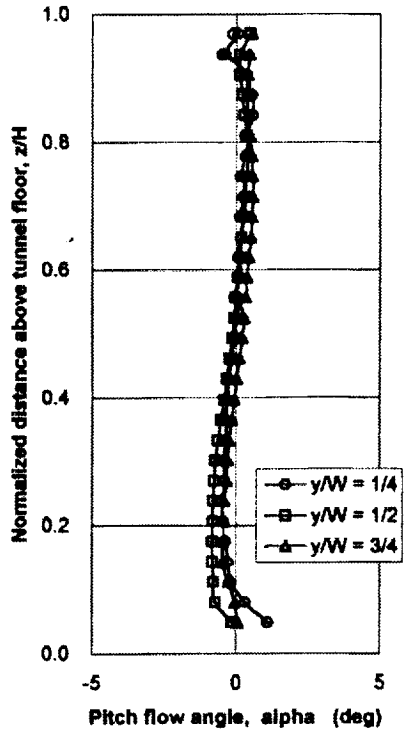

Figure 14 (b). Modified SMIRT pitch flow angles at Station 5: Spray Bar entrance plane.

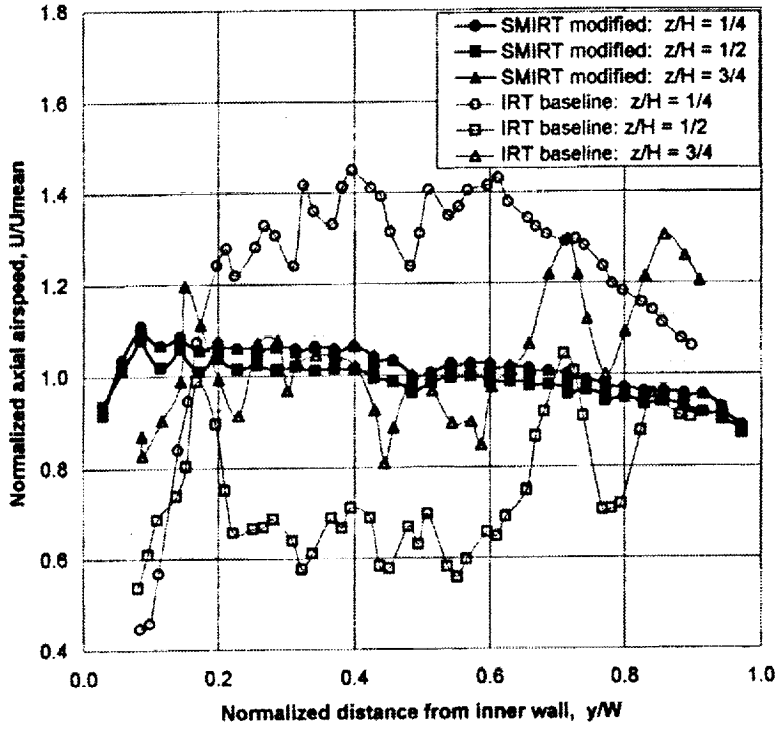

Figure 14 (c). Comparison of modified SMIRT and baseline IRT lateral airspeed distributions at Station 5: Spray Bar entrance plane.

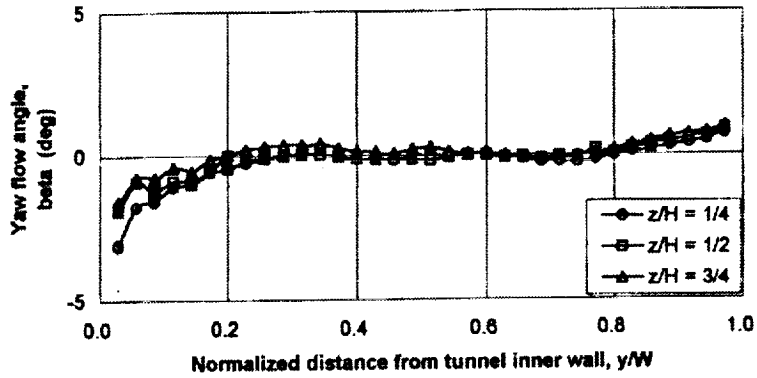

Figure 14 (d). Modified SMIRT yaw flow angles at Station 5: Spray Bar entrance plane.

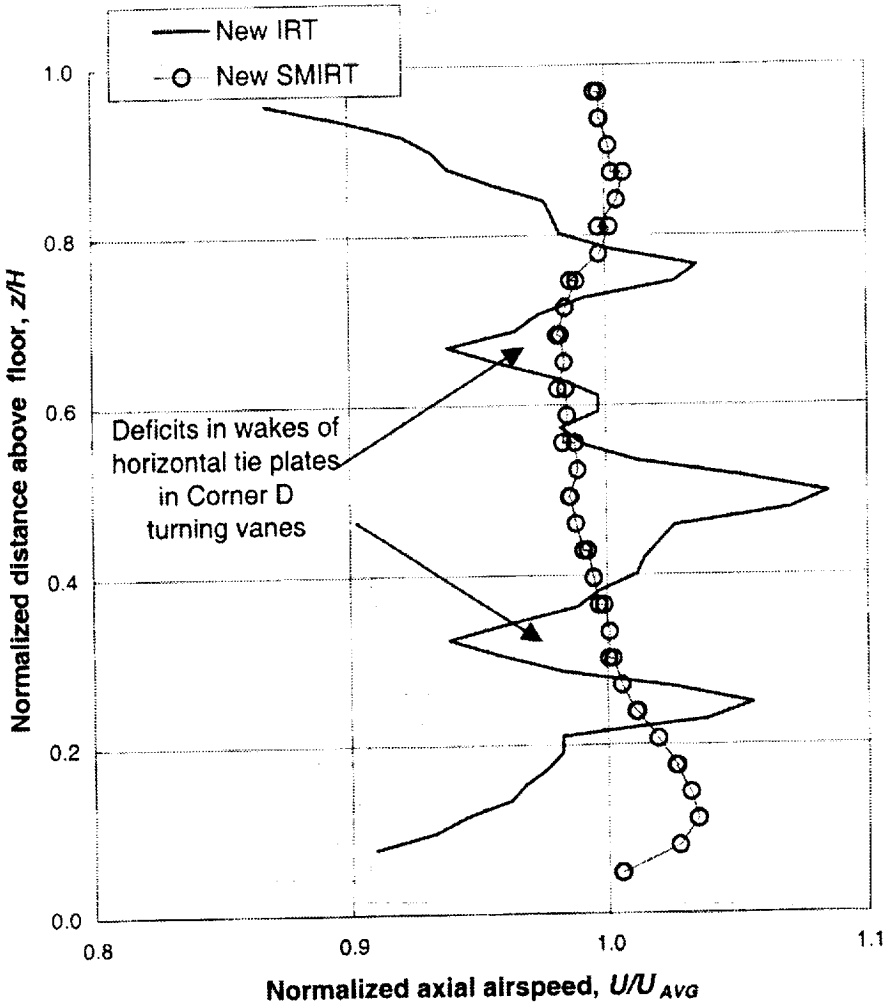

(a) Vertical distributions of axial airspeed along the tunnel centerline.

Figure 15. **Comparison of flow quality parameters in the Stilling Chambers of the modified IRT and the modified SMIRT (Station 5).**

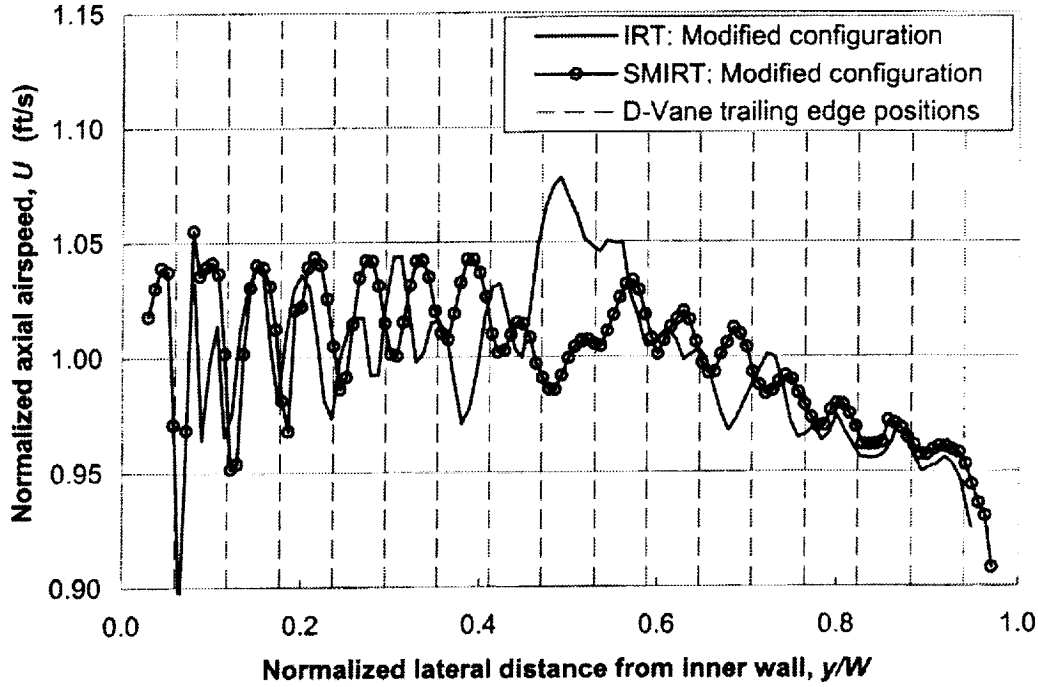

(b) Lateral distributions of axial airspeed at mid-elevation.

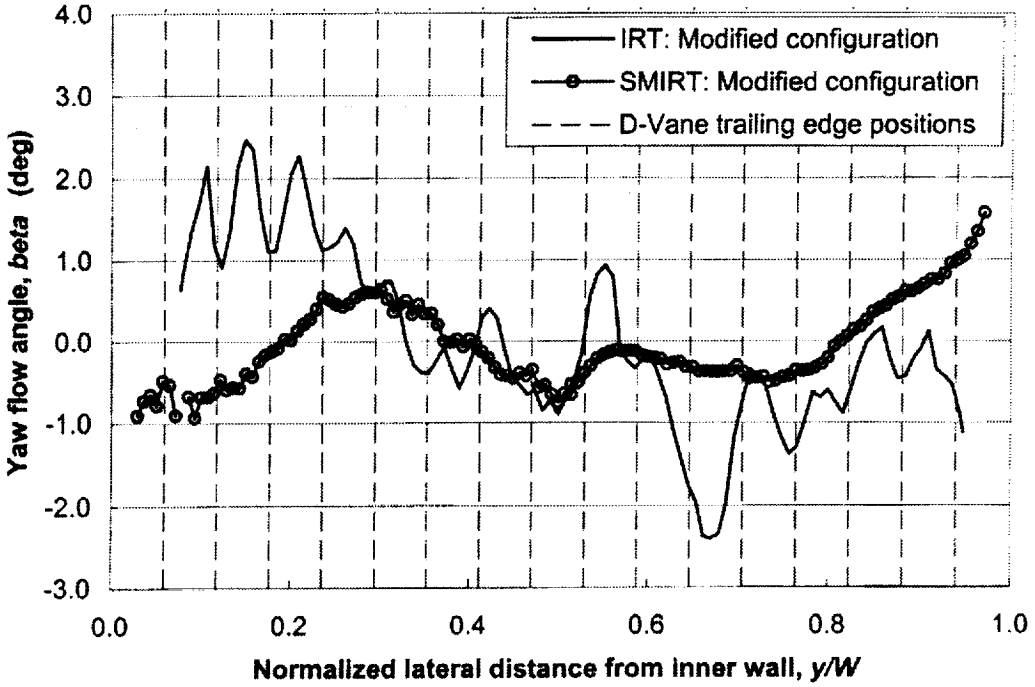

(c) Lateral distributions of yaw flow angle at mid-elevation.

Figure 15. Comparison of flow quality parameters in the Stilling Chambers of the modified IRT and the modified SMIRT (Station 5) (Continued).

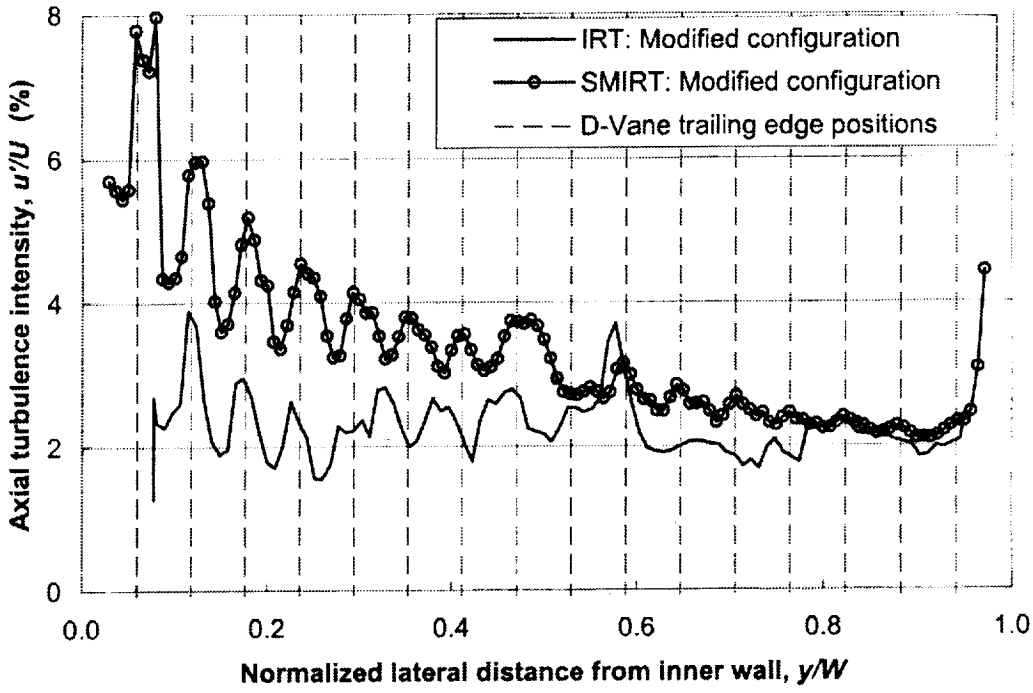

(d) Lateral distribution of axial turbulence intensity at mid-elevation.

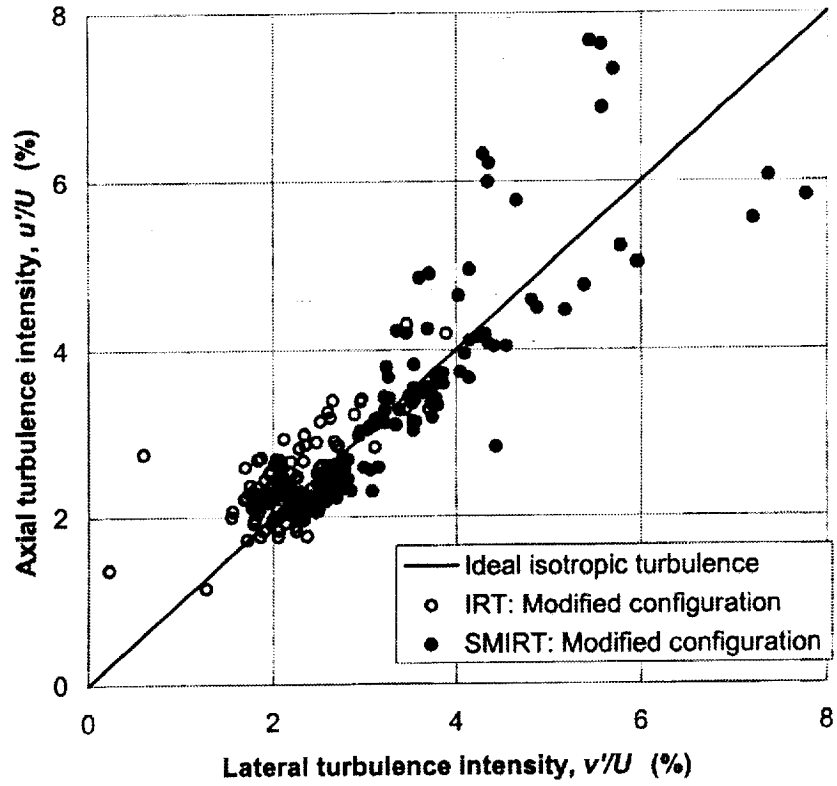

(e) Correlation of lateral and axial turbulence intensities.

Figure 15. Comparison of flow quality parameters in the Stilling Chambers of the modified IRT and the modified SMIRT (Station 5) (Concluded).

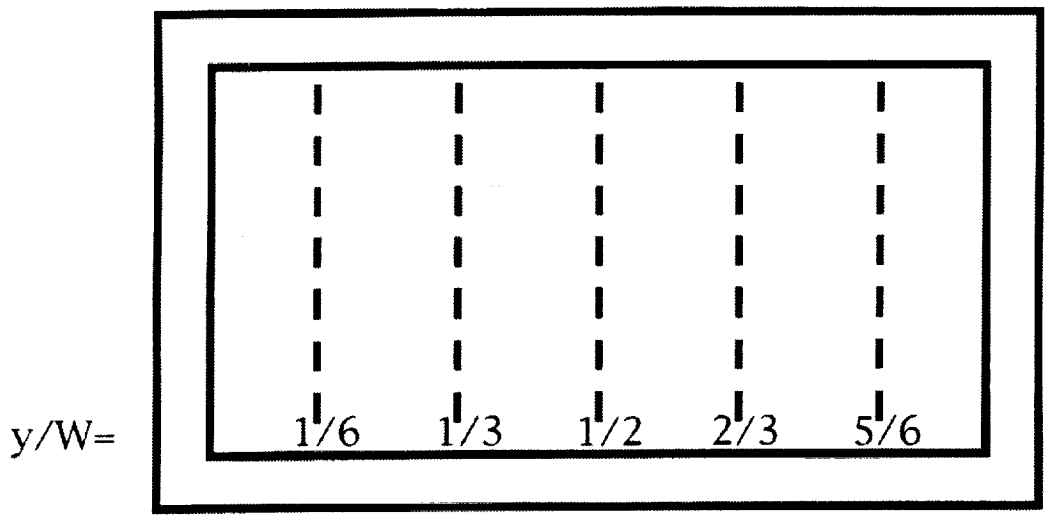

Test Section Area: 7.2 x 10.8 in.
Wall Thickness: 0.5 in.

Figure 16 (a). **SMIRT Test Section, downstream view, illustrating Vertical Traverse Locations - also see Figures 4 (f) and (g).**

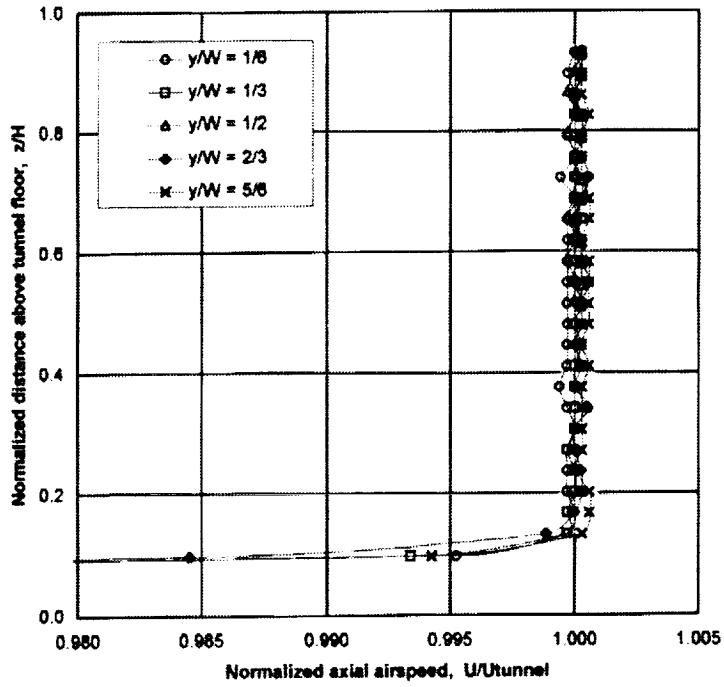

Figure 16(b). **Vertical distribution of axial airspeed across Station 6 in the Modified SMIRT: Mid-length of Test Section.**

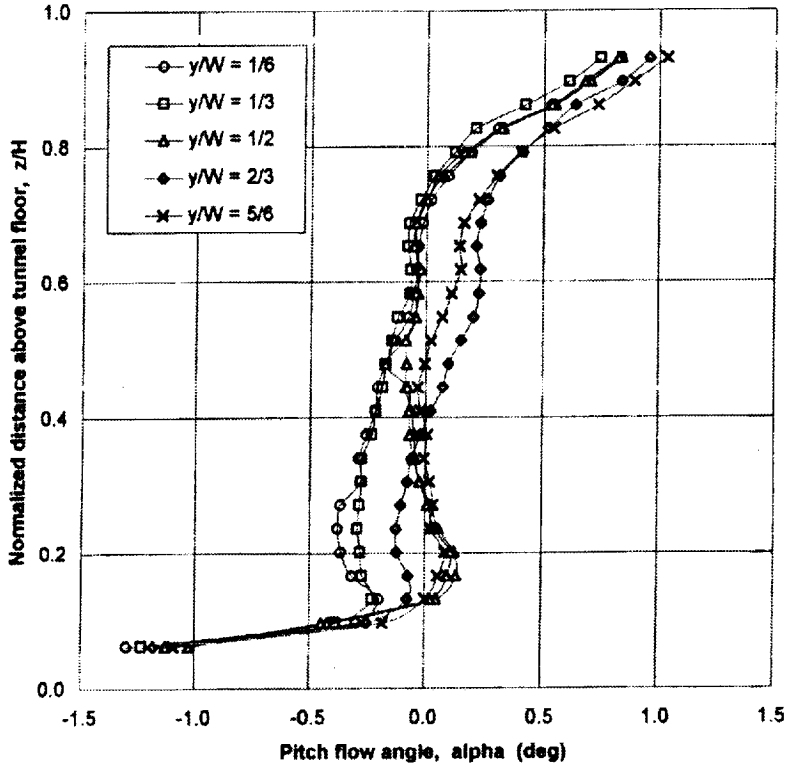

Figure 16 (c). **Vertical distribution of pitch flow angle in Modified SMIRT across Station 6: Mid-length of Test Section.**

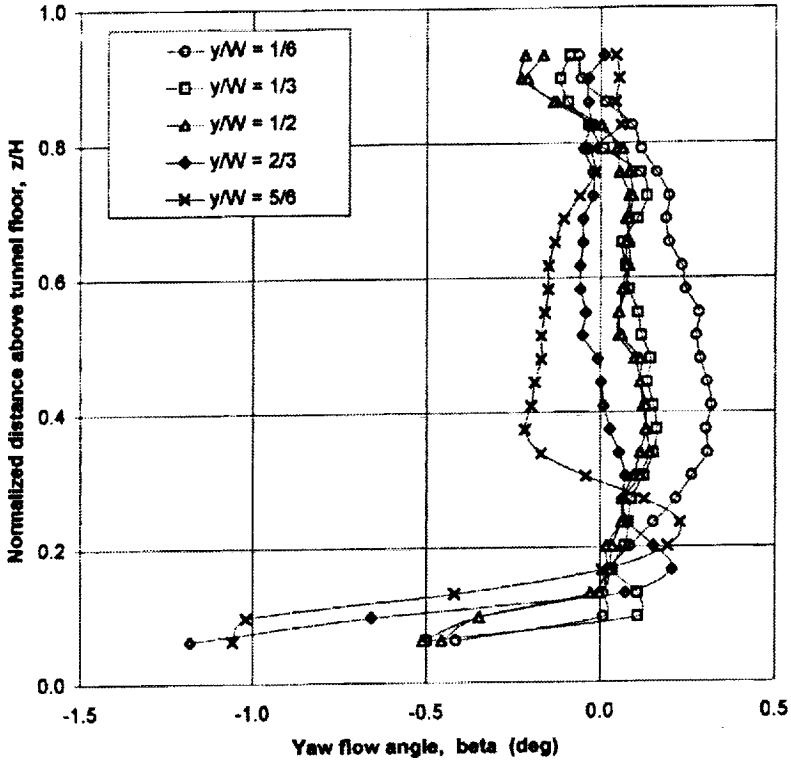

Figure 16 (d). **Vertical distribution of yaw flow angle in Modified SMIRT across Station 6: Mid-length of Test Section.**

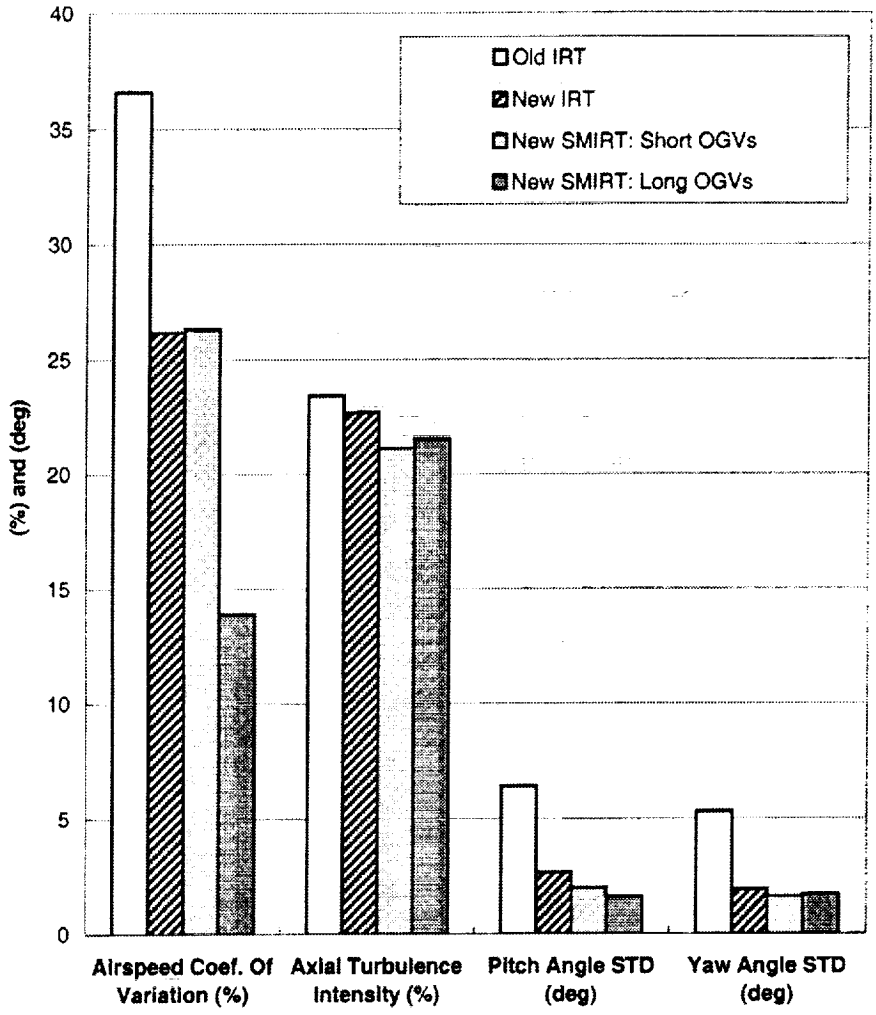

(a) Vent Tower Section (Station 2).

Figure 17. Bar charts comparing flow quality parameters measured in the IRT before and after modification with those measured in the modified SMIRT.

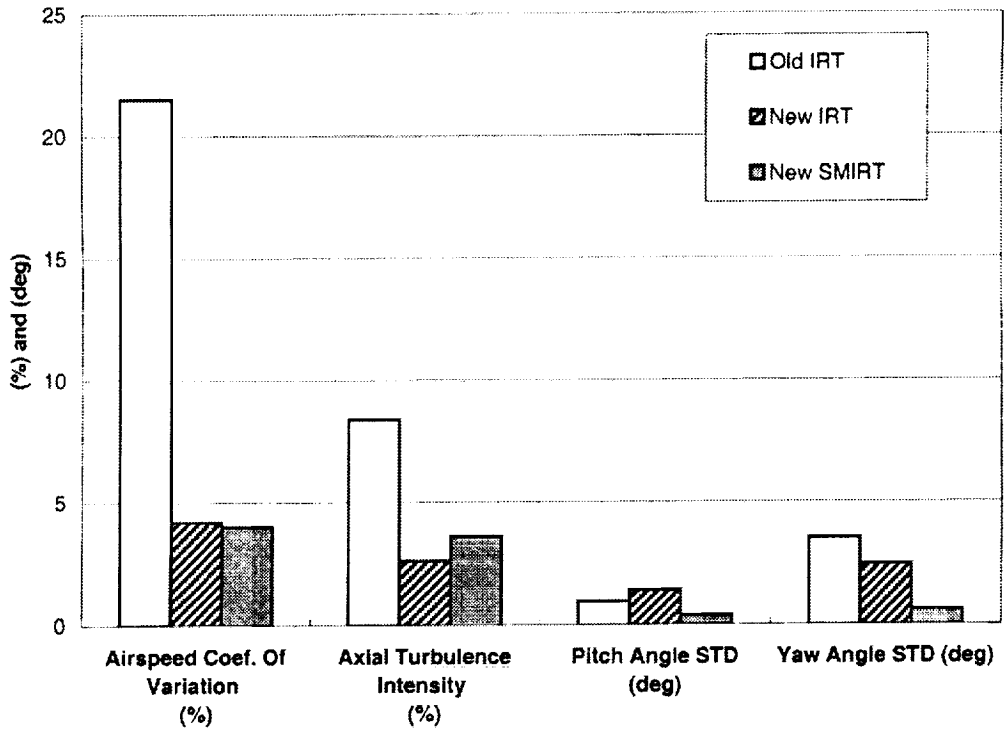

(b) Stilling Chamber Section (Station 5).

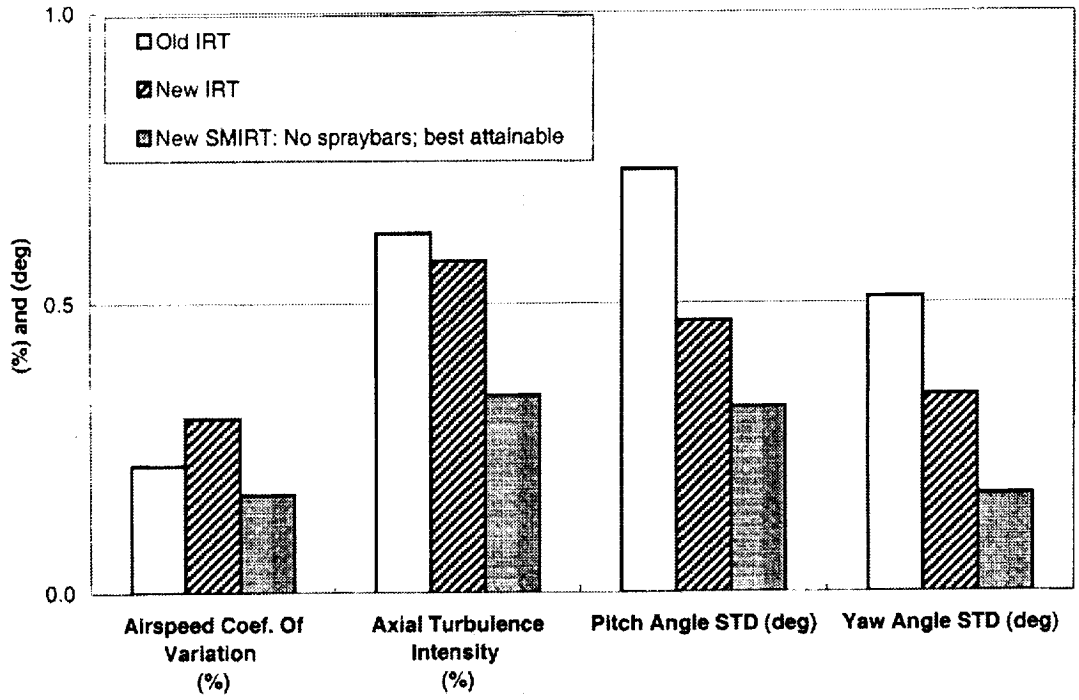

(c) Test Section, 4-ft x 5-ft zone (Station 6).

Figure 17. **Bar charts comparing flow quality parameters measured in the IRT before and after modification with those measured in the modified SMIRT (concl.).**

REPORT DOCUMENTATION PAGE

Form Approved
OMB No. 0704-0188

1. AGENCY USE ONLY (*Leave blank*)	2. REPORT DATE	3. REPORT TYPE AND DATES COVERED
	March 2001	Final Contractor Report

4. TITLE AND SUBTITLE

Use of a Scale Model in the Design of Modifications to the NASA Glenn Icing Research Tunnel

5. FUNDING NUMBERS

WU–708–90–1A–00
NAS3–98008

6. AUTHOR(S)

Victor A. Canacci, Jose C. Gonsalez, and David A. Spera

7. PERFORMING ORGANIZATION NAME(S) AND ADDRESS(ES)

Dynacs Engineering Company, Inc.
2001 Aerospace Parkway
Brook Park Ohio 44142

8. PERFORMING ORGANIZATION REPORT NUMBER

E–12614

9. SPONSORING/MONITORING AGENCY NAME(S) AND ADDRESS(ES)

National Aeronautics and Space Administration
Washington, DC 20546–0001

10. SPONSORING/MONITORING AGENCY REPORT NUMBER

NASA CR—2001-210687
AIAA–2001–0230

11. SUPPLEMENTARY NOTES

Prepared for the 39th Aerospace Sciences Meeting and Exhibit sponsored by the American Institute of Aeronautics and Astronautics, Reno, Nevada, January 8–11, 2001. Project Manager, Thomas Burke, Resources Analysis and Management Office, NASA Glenn Research Center, organization code 0210, 216–433–5172.

12a. DISTRIBUTION/AVAILABILITY STATEMENT

Unclassified - Unlimited
Subject Category: 09 Distribution: Nonstandard

Available electronically at http://gltrs.grc.nasa.gov/GLTRS

This publication is available from the NASA Center for AeroSpace Information, 301–621–0390.

12b. DISTRIBUTION CODE

13. ABSTRACT ***(Maximum 200 words)***

Major modifications were made in 1999 to the 6- by 9-Foot (1.8- by 2.7-m) Icing Research tunnel (IRT) at the NASA Glenn Research Center, including replacement of its heat exchanger and associated ducts and turning vanes, and the addition of fan outlet guide vanes (OGV's). A one-tenth scale model of the IRT (designated as the SMIRT) was constructed with and without these modifications and tested to increase confidence in obtaining expected improvements in flow quality around the tunnel loop. The SMIRT is itself an aerodynamic test facility whose flow patterns without modifications have been shown to be accurate, scaled representations of those measured in the IRT prior to the 1999 upgrade program. In addition, tests in the SMIRT equipped with simulated OGV's indicated that these devices in the IRT might reduce flow distortions immediately downstream of the fan by two thirds. Flow quality parameters measured in the SMIRT were projected to the full-size modified IRT, and quantitative estimates of improvements in flow quality were given prior to construction. In this paper, the results of extensive flow quality studies conducted in the SMIRT are documented. Samples of these are then compared with equivalent measurements made in the full-scale IRT, both before and after its configuration was upgraded. Airspeed, turbulence intensity, and flow angularity distributions are presented for cross sections downstream of the drive fan, both upstream and downstream of the replacement flat heat exchanger, in the stilling chamber, in the test section, and in the wakes of the new corner turning vanes with their unique expanding and contracting designs. Lessons learned from these scale-model studies are discussed.

14. SUBJECT TERMS

Wind tunnel; Subsonic; Scale model

15. NUMBER OF PAGES

47

16. PRICE CODE

A03

17. SECURITY CLASSIFICATION OF REPORT	18. SECURITY CLASSIFICATION OF THIS PAGE	19. SECURITY CLASSIFICATION OF ABSTRACT	20. LIMITATION OF ABSTRACT
Unclassified	Unclassified	Unclassified	